Cell Metabolism
Clinical and Translational Report

Canagliflozin impairs T cell effector function via metabolic suppression in autoimmunity

Graphical abstract

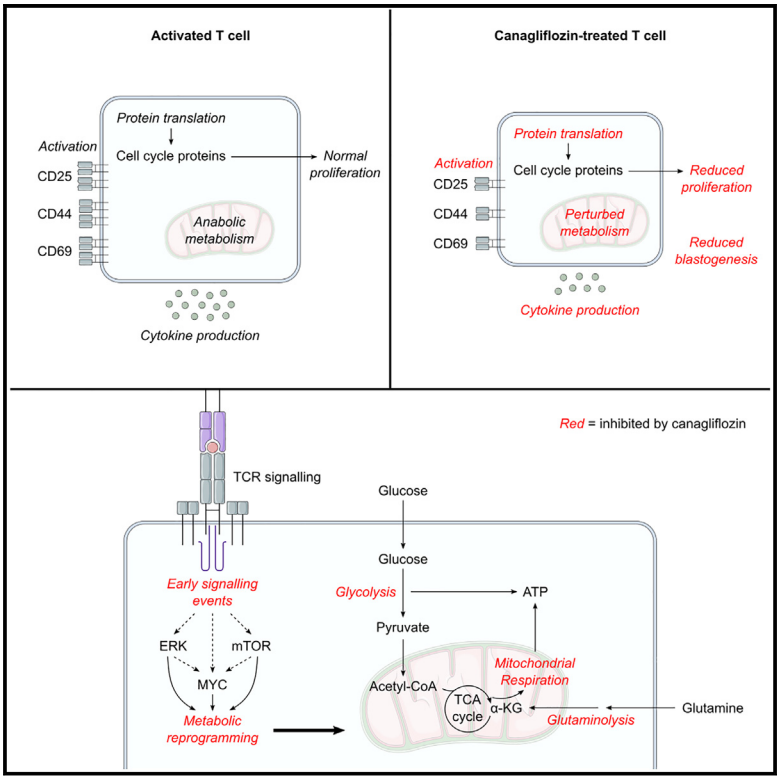

Highlights

- Canagliflozin (cana) inhibits human T cell effector function
- Cana compromises T cell receptor signaling
- Cana impairs the activity of ERK, mTORC, and Myc, preventing metabolic rewiring
- Cana impairs the effector function of T cells derived from patients with autoimmunity

Authors

Benjamin J. Jenkins, Julianna Blagih, Fernando M. Ponce-Garcia, ..., Linda V. Sinclair, Emma E. Vincent, Nicholas Jones

Correspondence

n.jones@swansea.ac.uk

In brief

Jenkins et al. report that the SGLT2 inhibitor, canagliflozin, compromises human T cell effector function. Canagliflozin prevents T cell activation and proliferation by antagonizing TCR signaling, impairing the activity of c-Myc, leading to a failure to engage in metabolic rewiring. *In vitro*, canagliflozin impairs T cell function in patients with autoimmunity.

Jenkins et al., 2023, Cell Metabolism *35*, 1–15
July 11, 2023
https://doi.org/10.1016/j.cmet.2023.05.001

CellPress

Cell Metabolism

CellPress
OPEN ACCESS

Clinical and Translational Report

Canagliflozin impairs T cell effector function via metabolic suppression in autoimmunity

Benjamin J. Jenkins,[1] Julianna Blagih,[2,3] Fernando M. Ponce-Garcia,[1] Mary Canavan,[4] Nancy Gudgeon,[5] Simon Eastham,[6] David Hill,[6] Megan M. Hanlon,[4] Eric H. Ma,[7,8] Emma L. Bishop,[5] April Rees,[1] James G. Cronin,[1] Elizabeth C. Jury,[9] Sarah K. Dimeloe,[5] Douglas J. Veale,[10] Catherine A. Thornton,[1] Karen H. Vousden,[2] David K. Finlay,[11] Ursula Fearon,[4] Gareth W. Jones,[6] Linda V. Sinclair,[12] Emma E. Vincent,[13,14] and Nicholas Jones[1,15,*]

[1]Institute of Life Science, Swansea University Medical School, Swansea University, Swansea SA2 8PP, UK
[2]The Francis Crick Institute, 1 Midland Road, London NW1 1AT, UK
[3]University of Montreal, Maisonneuve-Rosemont Hospital Research Centre, 5414 Assomption Blvd, Montreal, QC H1T 2M4, Canada
[4]Molecular Rheumatology, School of Medicine, Trinity Biomedical Sciences Institute, Trinity College Dublin, 152-160 Pearce Street, Dublin, Ireland
[5]Institute of Immunology and Immunotherapy, Institute of Metabolism and Systems Research, College of Medical and Dental Sciences, University of Birmingham, Birmingham, UK
[6]Cellular and Molecular Medicine, University of Bristol, Biomedical Sciences Building, Bristol BS8 1TD, UK
[7]Department of Metabolism and Nutritional Programming, Van Andel Institute, Grand Rapids, MI, USA
[8]Rheos Medicines, Cambridge, MA, USA
[9]Centre for Rheumatology Research, Division of Medicine, University College London, London, UK
[10]EULAR Centre of Excellence, Centre for Arthritis and Rheumatic Diseases, St Vincent's University Hospital, Dublin, Ireland
[11]School of Biochemistry and Immunology, Trinity Biomedical Sciences Institute, Trinity College Dublin, 152-160 Pearce Street, Dublin, Ireland
[12]Division of Cell Signalling and Immunology, School of Life Sciences, University of Dundee, Dundee, UK
[13]School of Translational Health Sciences, University of Bristol, Dorothy Hodgkin Building, Bristol BS1 3NY, UK
[14]Integrative Epidemiology Unit, School of Population Health Science, University of Bristol, Bristol BS8 2BN, UK
[15]Lead contact
*Correspondence: n.jones@swansea.ac.uk
https://doi.org/10.1016/j.cmet.2023.05.001

SUMMARY

Augmented T cell function leading to host damage in autoimmunity is supported by metabolic dysregulation, making targeting immunometabolism an attractive therapeutic avenue. Canagliflozin, a type 2 diabetes drug, is a sodium glucose co-transporter 2 (SGLT2) inhibitor with known off-target effects on glutamate dehydrogenase and complex I. However, the effects of SGLT2 inhibitors on human T cell function have not been extensively explored. Here, we show that canagliflozin-treated T cells are compromised in their ability to activate, proliferate, and initiate effector functions. Canagliflozin inhibits T cell receptor signaling, impacting on ERK and mTORC1 activity, concomitantly associated with reduced c-Myc. Compromised c-Myc levels were encapsulated by a failure to engage translational machinery resulting in impaired metabolic protein and solute carrier production among others. Importantly, canagliflozin-treated T cells derived from patients with autoimmune disorders impaired their effector function. Taken together, our work highlights a potential therapeutic avenue for repurposing canagliflozin as an intervention for T cell-mediated autoimmunity.

INTRODUCTION

Upon activation, human T cells adopt an anabolic metabolism to fuel the biosynthetic and energetic requirements of effector function.[1,2] This metabolic rewiring supports blastogenesis and the production of various immune-based mediators, such as cytokines, to drive the adaptive immune response.[3] One of the hallmarks of autoimmune disorders is aberrant T cell activation, which is supported by elevated metabolic demands.[4–6] For example, in rheumatoid arthritis (RA), patient-derived pathogenic T cells display dysregulated cellular metabolism underpinned by an enhanced requirement for energy and biosynthetic intermediates.[4,7,8] Furthermore, T cell metabolic rewiring, such as elevated glucose metabolism, lipid synthesis and glutaminolysis, and mitochondrial dysfunction, is a major driver of systemic lupus erythematosus (SLE) pathogenesis.[5,9,10] Taken together, these studies highlight that targeting the general immunometabolic profile of T cells could be therapeutically beneficial.

Appraising and repurposing type 2 diabetes (T2D) medications that target cellular metabolism as treatments for autoimmunity has significant potential.[11–15] For example, the biguanide and complex I inhibitor, metformin has been repurposed in RA,[16,17]

Please cite this article in press as: Jenkins et al., Canagliflozin impairs T cell effector function via metabolic suppression in autoimmunity, Cell Metabolism (2023), https://doi.org/10.1016/j.cmet.2023.05.001

SLE,[11,18] multiple sclerosis,[19,20] and myasthenia gravis.[21] In a recent clinical trial, metformin reduced the occurrence of severe flare-ups in patients with SLE.[11] Furthermore, the inhibitor rosiglitazone from the thiazolidinedione class suppressed pathogenic Th17-driven atopic dermatitis in obese mice.[22] These studies highlight the potential for targeting altered metabolic signatures characteristic of pathogenic T cells, using T2D drugs for therapeutic benefit in autoimmunity.

Sodium glucose co-transporter 2 (SGLT2) inhibitors are a novel class of T2D drugs approved for the treatment of T2D since 2012.[23] SGLT2 inhibitors, such as canagliflozin (cana) and dapagliflozin (dapa), target the SGLT2 transporter and prevent glucose reabsorption in the kidneys. Here, increased glucose excretion in the urine and a reduction in blood glucose improves glycemic control.[24,25] Interestingly, cana, as opposed to dapa, has been shown to have off-target effects, inhibiting mitochondrial glutamate dehydrogenase (GDH) and complex I.[26,27] Previous work has highlighted the beneficial effects of cana in renal and cardiovascular function in patients with chronic kidney disease and heart failure, respectively.[28,29] However, the effects of the gliflozins, specifically cana, on human T cell function is limited. As levels of SGLT2 are barely detectable in human T cells,[30] the aforementioned off-target effects of cana on mitochondria pose an interesting avenue to investigate in T cells.

Here, we found that cana but not dapa is a potent inhibitor of human T cell effector function. We reveal that in addition to the known off-target effects on GDH and complex I, cana inhibited T cell receptor (TCR) signaling resulting in compromised ERK and mTORC1 activity. These events were associated with a concomitant reduction in c-Myc levels, curbing metabolic reprogramming in activated T cells. This blunted metabolic response was associated with mitochondrial dysfunction, ultimately leading to impaired T cell effector function in multiple human T cell subsets. Importantly, cana was able to suppress T cell effector function in two autoimmune patient cohorts—SLE and RA—highlighting the potential of repurposing cana for improved treatment of T cell-mediated autoimmunity.

RESULTS

Canagliflozin modulates activated T cell function

We sought to better understand the effects of SGLT2 inhibitors on human CD4+ T cells—the key drivers in autoimmunity.[31] Here, we examined the effects of two different SGLT2 inhibitors; cana, which displays off-target effects on GDH and complex I, and dapa, which has no known off-target effects.[32] We purified human CD4+ naive T cells (Tnv) and activated them with anti-CD3 and anti-CD28 for 24 h in the presence or absence of physiologically relevant doses of either cana or dapa and assessed downstream effector function.[33,34] Cana significantly reduced IL-2 production in a dose-dependent manner, whereas dapa had a modest but non-significant effect (Figure 1A). This observation was not due to compromised cell viability (Figure 1B). Cana further constrained T cell activation by reducing expression of activation markers CD25, CD44, and CD69 (Figure 1C).

To confirm our findings in a more physiological setting, we utilized the recently developed human-plasma-like media (HPLM). The formulation of HPLM more accurately reflects the nutrient levels of human plasma and has profound effects on T cell function in comparison with traditional, non-physiological media, such as RPMI.[35] Once again, using HPLM, cana significantly impaired IL-2 production (Figure 1D) and activation marker expression (Figure 1E). Importantly, cana did not alter the phenotype of unstimulated Tnv based on measurement of activation markers (Figure S1A). These results demonstrate that cana treatment impairs T cell activation. Closer inspection of publicly available data (ImmGen [human] and ImmPRes [mouse]) indicate that SLC5A2 or "SGLT2" is minimally expressed in human T cells (normalized expression value of *SLC5A2* = 8, whereas *SLC2A1* (*GLUT1*) = 145, *SLC2A3* (*GLUT3*) = 277)[30] and undetectable in mouse T cells (www.immpres.co.uk). Taken together, this suggests that it is the "off-target" effects of cana rather than the known SGLT2 inhibitory effects that mediate inhibition of T cell activation programs.

Canagliflozin impairs T cell blastogenesis and proliferation

To better understand the impact of cana treatment on T cell function and phenotype, we next measured gene transcription in HPLM cultured, activated T cells. Using a NanoString human autoimmune panel, we revealed 3 downregulated and 39 upregulated genes upon cana treatment (Figure 2A). Our previous findings were confirmed at the gene transcript level with downregulation of *IL2* (Figure 2B). In contrast to our flow cytometry data, levels of the CD25 transcript, *IL2RA*, were significantly elevated upon cana treatment (Figure 2B) indicating potential issues at the translational level. We also observed significantly increased expression of *SELL* (CD62L; Figures 2B and S1B) in cana-treated cells compared with controls, which was also confirmed at the protein level (Figure S1C). These data also revealed that cana was associated with the downregulation of *CSF2* and *CCL20* genes—commonly associated with a Th17 signature[36] (Figure 2B). No significant transcript alterations were observed of T cells treated with dapa (Figure S1D).

Given the striking effects of cana on IL-2 production, we next assessed blastogenesis. Here, cana significantly reduced T cell blastogenesis (Figure 2C). This observation was in line with repressed downstream signaling targets involved in biogenesis, mainly mammalian target of rapamycin complex 1 (mTORC1). Two markers of mTORC1 activity, S6 ribosomal protein (S6) and 4E-BP1 phosphorylation, were both decreased at 4 and 24 h post-activation without changes in AMPK activity (a negative regulator of mTORC1[37]) and its downstream target acetyl-CoA carboxylase (Figures 2D and S1E).

To determine whether the effects of cana on T cells were long lived, we followed the activation of T cells out to 72 h of culture. Again, cana significantly reduced T cell proliferation (Figure 2E), IL-2 production, and STAT5 phosphorylation (Figures S1F and S1G) revealing that cana inhibits both short- and long-term T cell activation in physiological HPLM. Given the significant defects in IL-2 production in both HPLM and RPMI, we sought to identify whether the addition of exogenous IL-2 was able to rescue the observed phenotype. Supplementation with IL-2 did not rescue the cana-dependent effect on blastogenesis, indicating a more global effect on T cell suppression (Figure 2F).

Next, we assessed whether cana could suppress previously activated T cells and employed two strategies to determine this. First, we activated T cells for 48 h and subsequently

Please cite this article in press as: Jenkins et al., Canagliflozin impairs T cell effector function via metabolic suppression in autoimmunity, Cell Metabolism (2023), https://doi.org/10.1016/j.cmet.2023.05.001

Cell Metabolism
Clinical and Translational Report

CellPress
OPEN ACCESS

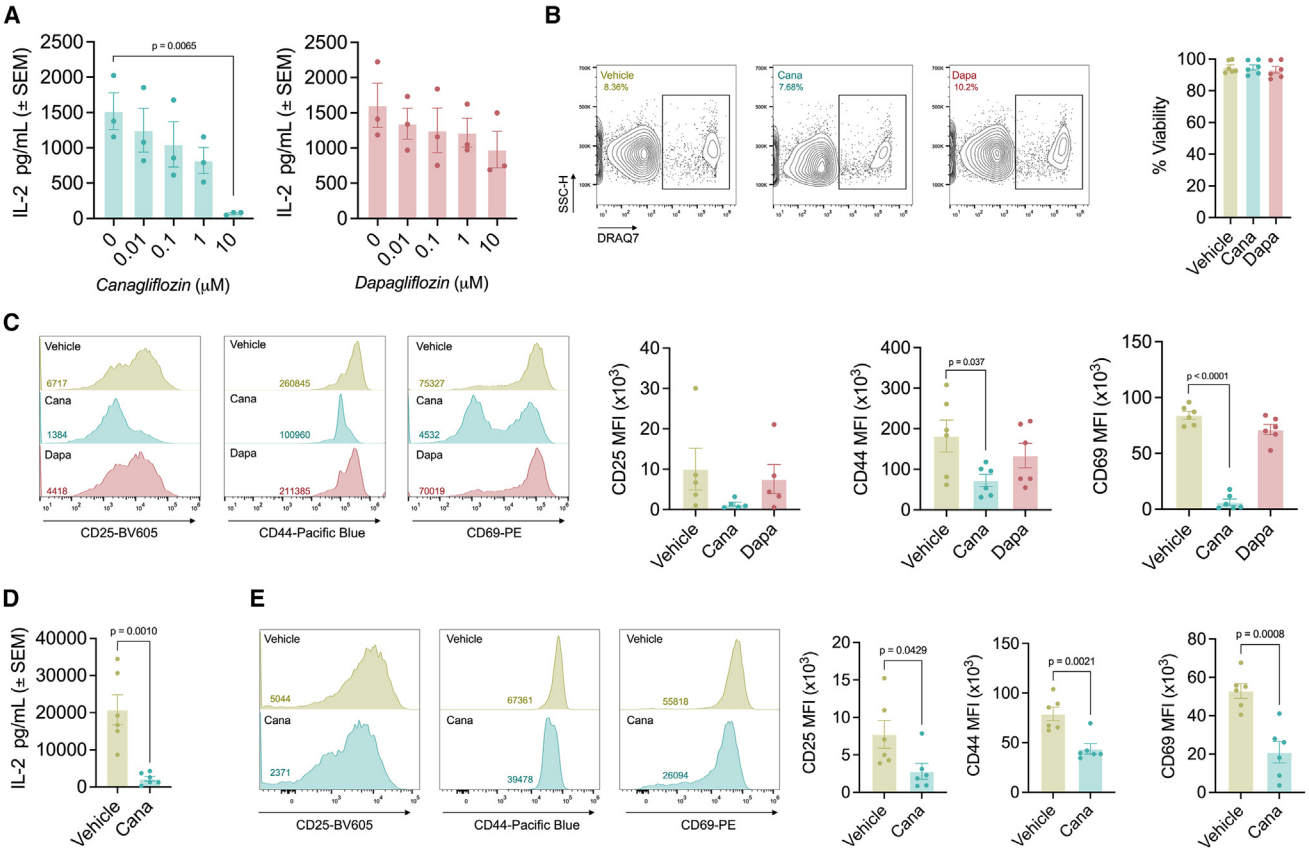

Figure 1. Canagliflozin impairs T cell activation

(A) Extracellular IL-2 release by anti-CD3 (2 μg/mL) and anti-CD28 (20 μg/mL) activated T cells treated with either canagliflozin or dapagliflozin at indicated concentrations for 24 h in RPMI.

(B) Activated T cell viability in the presence or absence of canagliflozin or dapagliflozin (both 10 μM). Representative contour plots, numbers indicate frequency of DRAQ7-positive cells.

(C–E) (C) Expression of activation markers CD25, CD44, and CD69. Representative overlaid histogram plots, numbers indicate median fluorescence intensity. T cells activated as (A) in HPLM media with (D) extracellular levels of IL-2 or (E) activation markers CD25, CD44, and CD69 assessed.

Data are representative of three (A), six (B, D, and E), or five-six (C) independent experiments. Data are expressed as mean ± SEM.

See also Data S2.

introduced cana for the final 24 h of culture. Here, cana retained an ability to reduce blastogenesis in activated T cells (Figures S1H and S1I). Second, we activated purified total or "pan" CD4+ T cells for 24 h, treating them for a further 72 h (supplemented with IL-2) with increasing doses of cana. Here, cana was able to suppress total CD4+ T cell counts and a reducing trend in IFNγ production, but at higher concentrations than those when starting from a naive T cell population (Figures S1J and S1K). Taken together, our data demonstrate that cana suppresses T cell activation in a physiological environment.

Canagliflozin suppresses c-Myc signaling

To better understand the underlying mechanisms responsible for the impact of cana treatment on activated T cells, we assessed immunometabolic changes at the gene transcript level. Using a NanoString human metabolism panel we revealed that cana treatment resulted in 24 downregulated and 14 upregulated genes (Figure 3A). Pathway analysis of downregulated genes identified functions linked to glycolysis, c-Myc, and cell cycle, which supported our earlier findings (Figures 3B and 3C). At the transcript level, *c-Myc* expression was unaffected (Figure 3D), whereas it was reduced at the protein level upon cana treatment at both an early (4 h) and late time point (24 h), indicating a translational rather than transcriptional perturbation (Figure 3E).

As c-Myc is a master transcription factor, integral to metabolic reprogramming of T cells upon activation,[38,39] we explored our findings further by carrying out label-free liquid chromatography-mass-spectrometry-based whole-cell proteomics to investigate the impact of cana on the global activated T cell proteome. In line with cana reducing cell size (Figure 2C), cana-treated cells had a significantly lower protein mass in comparison with those treated with the vehicle control (Figure 3F). A total of 5,655 proteins were detected and differential expression analysis revealed that at the copy-number level, 4,421 proteins were significantly reduced whereas one protein was upregulated—the cell-cycle inhibitor, CDKN1B (Figures 3G and S2A). Importantly, we were not able to detect SLC5A2 or SGLT2 in

Please cite this article in press as: Jenkins et al., Canagliflozin impairs T cell effector function via metabolic suppression in autoimmunity, Cell Metabolism (2023), https://doi.org/10.1016/j.cmet.2023.05.001

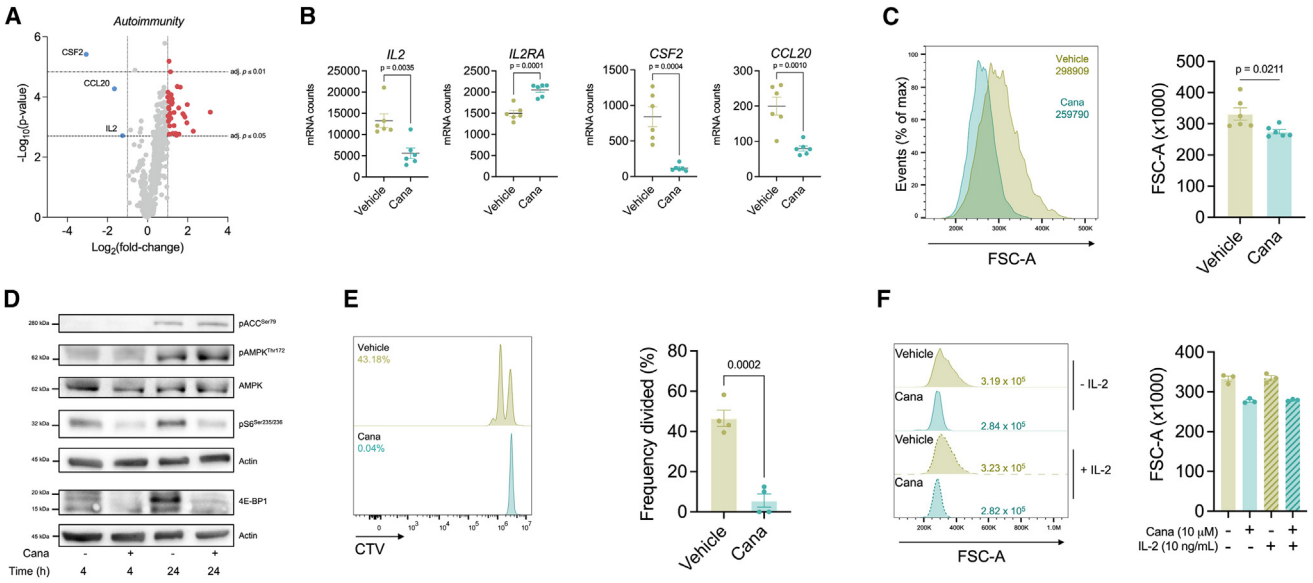

Figure 2. Canagliflozin inhibits T cell proliferation

T cells were activated with anti-CD3 (2 μg/mL) and anti-CD28 (20 μg/mL) and treated with or without canagliflozin (10 μM) for 24 h.

(A) NanoString differential expression analysis of autoimmunity-associated genes in canagliflozin-treated T cells versus vehicle control. Blue and red data points represent downregulated and upregulated genes, respectively. Genes with an adjusted p value < 0.05 and $\log_2$ fold-change <−1 and >1 were considered differentially expressed.

(B) Normalized mRNA counts for *IL2*, *IL2RA*, *CSF2*, and *CCL20*.

(C) T cell blastogenesis levels with representative overlaid histogram plots, numbers indicate FSC-A.

(D) Immunoblot of phospho-acetyl-CoA carboxylase (pACC), phospho-AMPK, AMPK, phospho-S6 ribosomal protein, 4E-BP1 and β-actin assessment in activated CD4+ T cells at 4 and 24 h.

(E) T cell proliferation measured by flow cytometry using CTV on cells activated with anti-CD3 (2 μg/mL) and anti-CD28 (20 μg/mL) for 72 h.

(F) Tnv activated for 24 h ± IL-2 (10 ng/mL) in the presence or absence of canagliflozin (10 μM) with representative overlaid histogram plots, numbers indicate FSC-A.

Data are representative of six (A–C), four-five (D), four (E), or three (F) independent experiments. Data are expressed as mean ± SEM.

See also Data S1 and S2.

our proteomic dataset. We next took into consideration the concentration of the detected proteins, irrespective of cell size. Here, 481 proteins were downregulated in response to cana treatment, while 203 proteins were upregulated ($\log_2$ fold-change of ±0.585, p value ≤ 0.05; Figures 3H and S2A). Of these downregulated proteins, we confirmed that c-Myc was significantly reduced at both the copy-number and concentration level (Figure 3I).

To better understand the biological relevance of these protein changes, ingenuity pathway analysis (IPA) was employed to consider the contribution of individual proteins toward various canonical cellular pathways and their enrichment following cana treatment. Here, "cell-cycle control of chromosomal replication" emerged as the most significantly downregulated pathway, supporting the observed effects on T cell proliferation (Figure 3J). Given the known effects of cana on mitochondrial proteins (GDH and complex I), it was not surprising that "oxidative phosphorylation (OXPHOS)" and "mitochondrial dysfunction" were the predominant upregulated pathways in cana-treated T cells (Figure 3K). Cana treatment resulted in the compensatory enrichment of several ETC complex-associated proteins, with concomitant increases in mitochondrial mass and membrane potential as determined by flow cytometry (Figures S2B–S2D). Concomitant with mitochondrial dysfunction, other upregulated pathways included proteins associated with "sirtuin signaling" and "glutathione redox reactions" (Figure 3K), which was consistent with elevated early mitochondrial ROS production (Figure S2E) and heightened levels of proteins associated with the response to oxidative stress (Figures S2F–S2J) in cana-treated T cells.

Subsequent analysis allowed us to identify potential upstream regulators (e.g., transcription factors, microRNAs, kinases, small molecule inhibitors) associated with changes in the activated T cell proteome following cana treatment. Here, the activation *Z* score predicts the activation state of each predicted upstream regulator. In line with our NanoString and immunoblot data, reduced expression of 52 distinct targets predicted that c-Myc might be an upstream regulator which is repressed following cana treatment (Figure 3L). Interestingly, the drug torin1 and protein RICTOR—important upstream regulators of the mTOR axis—were identified as potential upstream regulators that were suppressed based on proteins upregulated in cana-treated T cells (Figure 3M).

Given the agreement between transcriptional and proteomic analysis on c-Myc-associated pathways, we further interrogated the proteomics dataset and observed several c-Myc-associated metabolic targets that were significantly inhibited with cana treatment including SLC2A1 (GLUT1), hexokinase 2 (HK2),

Please cite this article in press as: Jenkins et al., Canagliflozin impairs T cell effector function via metabolic suppression in autoimmunity, Cell Metabolism (2023), https://doi.org/10.1016/j.cmet.2023.05.001

Cell Metabolism
Clinical and Translational Report

CellPress
OPEN ACCESS

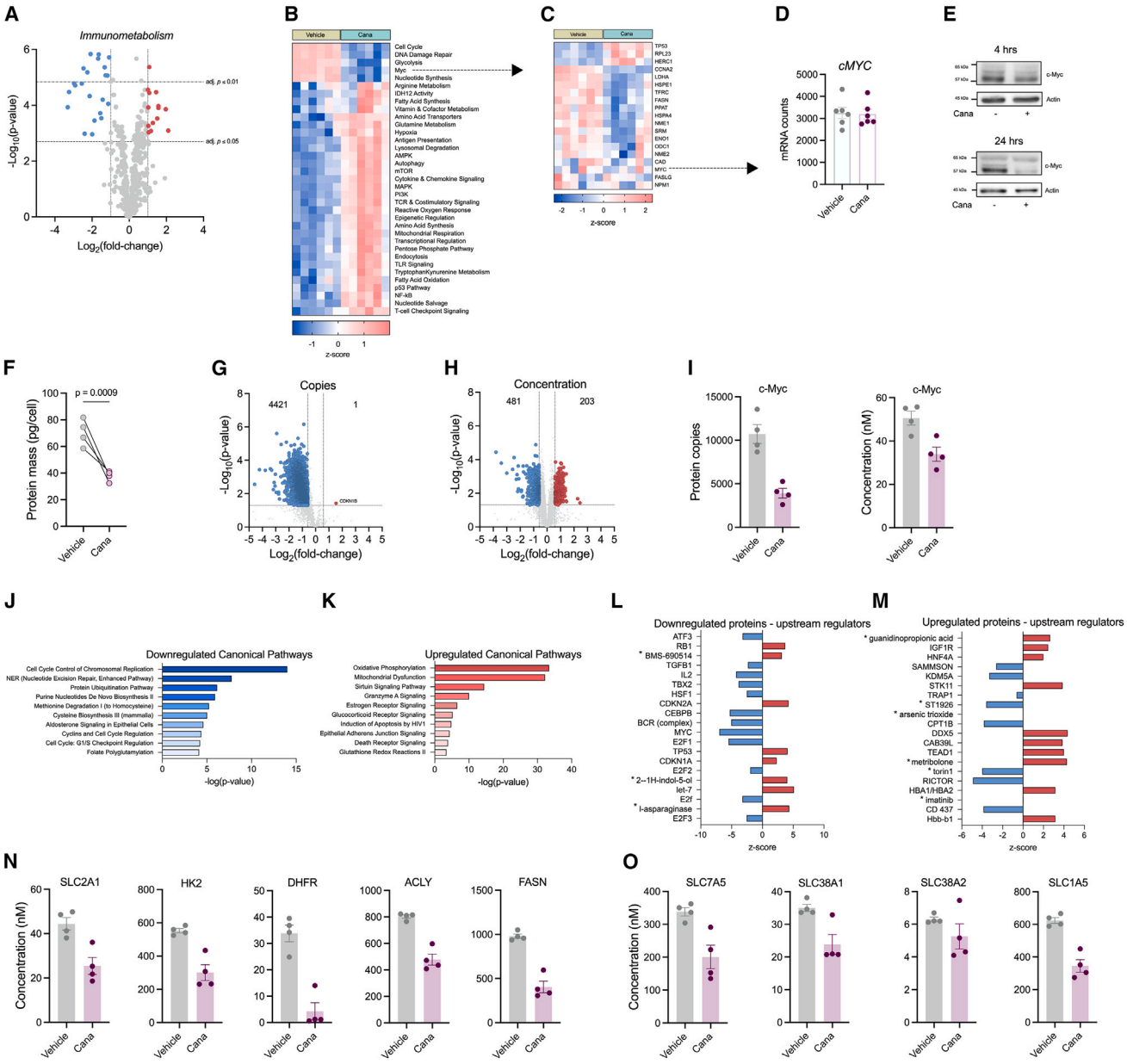

Figure 3. Canagliflozin remodels the T cell proteome

(A) NanoString human immunometabolism panel—differential expression analysis of metabolism-associated genes in canagliflozin-treated activated T cells versus vehicle control. Blue and red data points represent downregulated and upregulated genes, respectively. Genes with an adjusted p value < 0.05 and $\log_2$ fold-change <−1 and >1 were considered differentially expressed.

(B and C) (B) Hierarchical clustering of pathway *Z* scores with (C) c-Myc target genes.

(D) Normalized mRNA counts for c-*myc*.

(E) c-Myc assessment in pan CD4+ T cells activated with anti-CD3 (2 μg/mL) and anti-CD28 (20 μg/mL) and treated with or without canagliflozin (10 μM) for 4 and 24 h by immunoblot.

(F) Total cellular protein content in cana-treated activated T cells versus vehicle control.

(G and H) Differential expression analysis of proteins by label-free mass spectrometry in canagliflozin-treated activated T cells versus vehicle control, based on (G) protein copies and (H) protein concentration. Blue and red data points represent downregulated and upregulated genes, respectively. Proteins with an adjusted p value < 0.05 and $\log_2$ fold-change > 0.585 were considered differentially expressed.

(I–M) (I) c-Myc protein expression as determined by number of copies and concentration. Ingenuity pathway analysis (IPA) of canonical pathways based on significantly (J) downregulated and (K) upregulated proteins. Top 10 enriched pathways are shown. Analysis of predicted upstream regulators in IPA based on significantly (L) downregulated or (M) upregulated proteins, Asterisk (*) denotes a chemical drug of which cana is predicted to respond in a similar fashion at the

(legend continued on next page)

Please cite this article in press as: Jenkins et al., Canagliflozin impairs T cell effector function via metabolic suppression in autoimmunity, Cell Metabolism (2023), https://doi.org/10.1016/j.cmet.2023.05.001

dihydrofolate reductase (DHFR), ATP citrate lyase (ACLY), and fatty acid synthase (FASN) (Figure 3N) and solute transporters SLC7A5, SLC38A1, SLC38A2, and SLC1A5 (Figures 3O and S2K). In fitting with a reduction in c-Myc activity, we observed significant decreases in translational machinery in concert with no difference in the concentration of the translational inhibitor, PDCD4 (Figures S2L–S2R). Collectively, these data demonstrate that cana treatment blunts c-Myc signaling and results in concomitant mitochondrial dysfunction, leading to impaired T cell metabolism and function.

Canagliflozin impairs TCA cycle metabolism via GDH inhibition

Given that cana blunts c-Myc induction, we next sought to directly measure cellular metabolism in response to cana treatment. We activated naive CD4+ T cells for 24 h in the presence or absence of cana and monitored metabolic alterations using a mitochondrial stress assay. Interestingly, cana perturbed the extracellular acidification rate (ECAR; Figures 4A, S3A, and S3B) and oxygen consumption rates (OCRs; Figures 4B and S3C–S3F). Specifically, cana reduced adenosine triphosphate (ATP) production from glycolysis (Figure 4C) and affected the maximal respiration rates leading to a significant drop in ATP production from OXPHOS (Figure 4D). Moreover, cana significantly reduced the bioenergetic scope of activated T cells by impacting on their ability to generate ATP at the maximal rate (Figures S3G and S3H). No metabolic perturbation was observed in activated T cells treated with dapa (Figures S3G and S3H). Furthermore, activated T cells and effector T cells (Teff) cells in the presence of cana released significantly lower levels of lactate in comparison with the vehicle or dapa-treated cells (Figures S3I and S3J). Taken together, these results indicate that it is the off-target effects of cana that perturb T cell metabolism rather than the ''on-target'' effects of SGLT2 inhibition.

Given the clear metabolic effects of cana on activated T cells, we next employed liquid chromatography-mass spectrometry (LC-MS/MS) to track cellular metabolites. The total abundance of individual tricarboxylic acid (TCA) cycle intermediates was reduced in the presence of cana (Figure 4E), while levels of the amino acids, glutamate, and aspartate were unchanged (Figure 4F). To determine whether cana inhibits GDH in activated T cells, we performed stable isotope labeling using a uniformly labeled $^{13}C_5$-glutamine (Gln) probe to measure the incorporation of Gln-derived carbon through GDH and into the TCA cycle (Figure 4G). Total intracellular levels of ^{13}C-Gln and ^{13}C-αKG were reduced in cana-treated T cells, while there was no impact on ^{13}C-glutamate abundance, indicating impaired Gln uptake and inhibition at GDH (Figure 4H). When we analyzed the total proportion of ^{13}C incorporation into metabolite pools irrespective of mass isotopolog distribution, levels of ^{13}C into αKG and citrate were significantly reduced with cana (Figure 4I). Furthermore, levels of incorporation of ^{13}C into the m + 5 mass isotopolog of αKG were significantly reduced with cana treatment (Figure 4J). This trend was apparent in other TCA cycle metabolites, including amino acids, glutamate, aspartate, and proline (Figures S3K–S3M). In an attempt to rescue the effect of cana-mediated GDH inhibition, we cultured cells with membrane-permeable αKG; however, this did not restore IL-2 production in cana-treated T cells (Figure 4K).

As metabolic perturbation is associated with plasticity in human T cells,[1] we next wanted to determine the impact of the impaired glutamine utilization on $^{13}C_6$-glucose metabolism (Figure S3N). Cana treatment impaired lactate production from glucose, as illustrated by a reduction in the lactate m + 3 isotopolog (Figure S3O), consistent with the reduced ECAR we observed (Figure 4A). Analysis of the total ^{13}C incorporation into metabolite pools revealed significant increases in malate, glutamate and aspartate (Figure S3P). Consistent with this, cana promoted the entry of glucose-derived carbon into the TCA cycle (Figure S3Q) and amino acid (glutamate and aspartate) metabolite pools (Figure S3R). These data suggest that T cells metabolically adapt to cana-induced GDH inhibition by becoming more reliant on glucose-derived TCA cycle intermediates.

To determine whether the effects observed can be explained by inhibition of complex I, another known off-target effect of cana, we activated T cells in the presence or absence of cana, alongside other known complex I inhibitors—rotenone and high-dose metformin (to bypass any transporter-specific uptake). Cana was the superior T cell inhibitor when assessing IFNγ release, CD69 expression, and blastogenesis (Figures S3S–S3U) in comparison with rotenone or metformin. Given this, we next considered whether the combined effect of complex I and GDH inhibition might underpin the impaired effector function of T cells. Therefore, we activated T cells in the presence or absence of cana, piericidin A (an alternative complex I inhibitor), R162 (GDH inhibitor) or in combination. Cana was again, the most effective T cell inhibitor when assessing IFNγ release (Figure 4L), CD69 expression (Figure 4M), and blastogenesis (Figure 4N) in comparison with piericidin A, R162, or the combination treatment. These data suggest that inhibition of complex I and GDH are not the sole drivers in T cell dysregulation downstream of cana treatment.

Canagliflozin impairs T cell receptor signaling

We have demonstrated that cana significantly impacts on key intracellular metabolic nodes—mTOR and c-Myc. As both signaling molecules are sensitive to downstream signals from the TCR,[40] we sought to investigate the role of cana on T cell signaling. Here, we cultured T cells in the presence or absence of cana and assessed the early signaling events downstream of the TCR in ZAP70, LAT, and PLCγ. Cana impaired phosphorylation of all TCR targets assessed (Figure 5A) and subsequently blunted ERK phosphorylation in line with a MAPK inhibitor

protein level. The *Z* score predicts the likely activation states of upstream regulators; a positive *Z* score suggests activation, while a negative *Z* score suggest inhibition.

(N) c-Myc targets assessed via upstream analysis of the proteomics dataset.

(O) Concentration of c-Myc-associated amino acid transporters SLC7A5, SLC38A1, SLC38A2, and SLC1A5.

Data are representative of six (A–D), three-four (E), and four (F–O) independent experiments. Data are expressed as mean ± SEM.

See also Data S1 and S2.

Please cite this article in press as: Jenkins et al., Canagliflozin impairs T cell effector function via metabolic suppression in autoimmunity, Cell Metabolism (2023), https://doi.org/10.1016/j.cmet.2023.05.001

CellPress
OPEN ACCESS

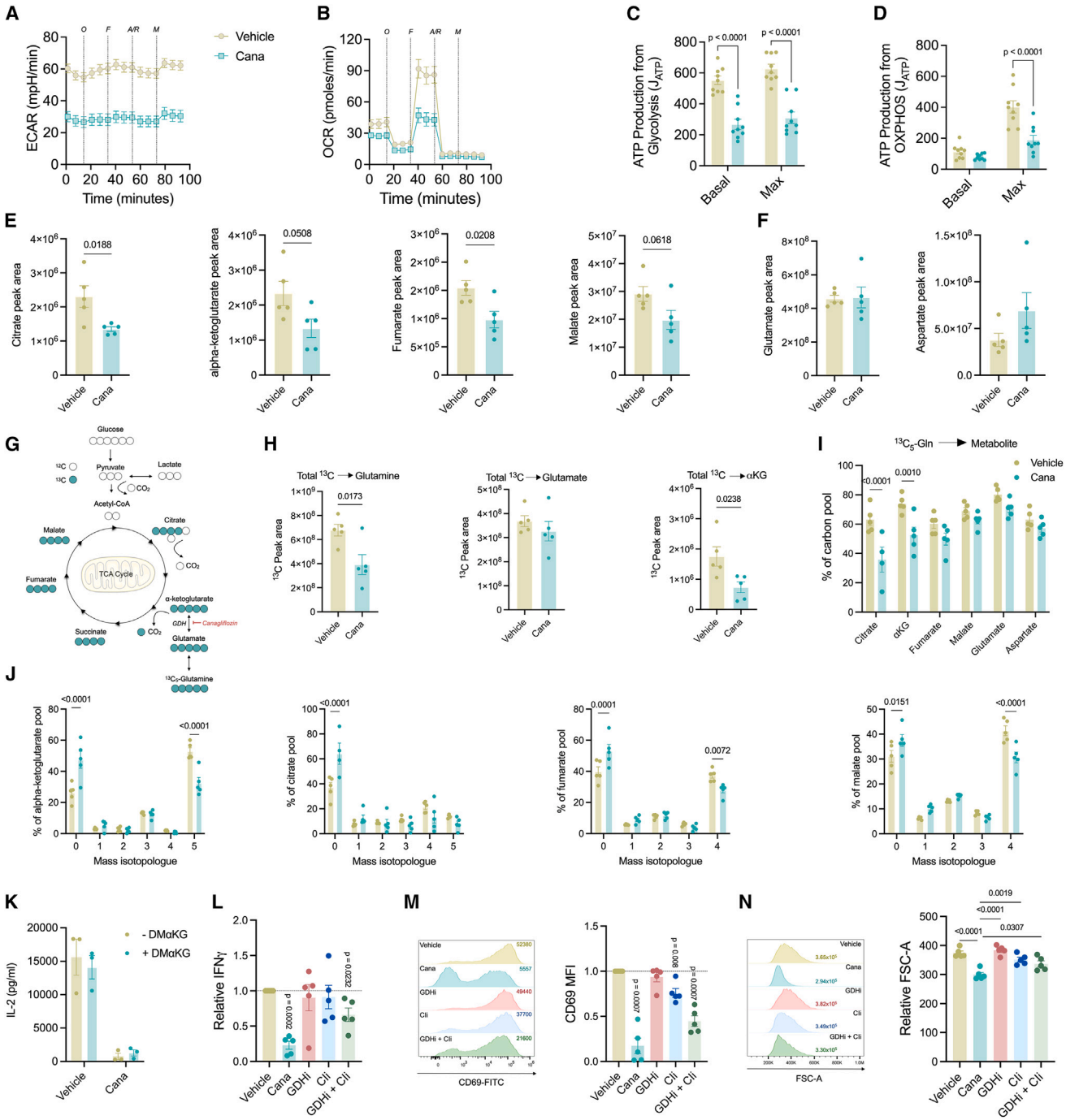

Figure 4. Canagliflozin inhibits glutamine anaplerosis toward the TCA cycle

(A–D) Seahorse extracellular flux analysis of (A) extracellular acidification rate (ECAR) or (B) oxygen consumption rate (OCR) in 24 h activated T cells following pre-optimized injections of oligomycin, FCCP, antimycin A/rotenone (all 1 μM), and monensin (20 μM). Basal or maximal ATP production (J_{ATP}) from (C) glycolysis or (D) OXPHOS.

(E–G) (E) Total ion count of TCA cycle metabolites: citrate, α-ketoglutarate, fumarate, malate, and (F) amino acids: glutamate and aspartate of 8 h activated (anti-CD3 [2 μg/mL] and anti-CD28 [20 μg/mL]) T cells treated with or without canagliflozin (10 μM) (G) Schematic of stable isotope tracing of uniformly labeled ^{13}C-glutamine into the TCA cycle.

(H) Total ^{13}C incorporation (peak area) of metabolites glutamine, glutamate, and α-ketoglutarate.

(I) Relative abundance of ^{13}C-glutamine to derived metabolites: citrate, α-ketoglutarate, fumarate, malate, glutamate, and aspartate.

(legend continued on next page)

Please cite this article in press as: Jenkins et al., Canagliflozin impairs T cell effector function via metabolic suppression in autoimmunity, Cell Metabolism (2023), https://doi.org/10.1016/j.cmet.2023.05.001

(Figure 5B). In addition, cana-treated cells showed delayed CD69 expression (downstream ERK target; Figure 5C). Given the impact of cana on TCR signaling, we sought to determine whether cana would affect human CD8+ T cells in the same manner. Here, cana significantly suppressed blastogenesis, activation marker expression and IL-2, IFNγ and granzyme B production in CD8+ T cells (Figures S4A–S4D).

Next, we tested whether the impaired TCR signaling caused by cana was responsible for the observed defects in cytokine production. In an attempt to rescue cytokine production, we stimulated T cells with the diacylglycerol (DAG) mimetic—PMA and ionomycin—in order to bypass the TCR, and thus any downstream effects of cana on the TCR. T cells treated with PMA/ionomycin in the presence of cana did not have any defect in cytokine production in comparison with the vehicle control (Figure 5D).

Given the dysregulation of critical signaling nodes (ERK and mTORC1) by cana, we hypothesized that cana treatment would phenocopy inhibition of these nodes. Here, we treated T cells with cana, rapamycin (mTORC1 inhibitor) and a MAPK inhibitor (ERK inhibition) and measured early (4 h) c-Myc expression and early (4 h) and late (24 h) puromycin incorporation (a measure of translation). Here, cana phenocopied both mTORC1 and MAPK inhibition by reducing c-Myc expression (Figure 5E) and puromycin incorporation at both 4 and 24 h (Figures 5F and 5G). Functionally, cana phenocopied both mTORC1 and ERK inhibition by significantly reducing blastogenesis (Figure 5H) and IFNγ production (Figure 5I). Taken together, these data suggest that, mechanistically, cana impairs TCR signaling leading to suppressed signaling to metabolic nodes. Additionally, the data indicate that c-Myc protein expression is downstream of ERK and mTORC1 signaling in TCR activated human T cells.

Canagliflozin inhibits the diverse cytokine profile of T effector cells

Thus far, we have shown that cana inhibits the function of activated T cells that display a restricted cytokine profile. To determine if cana suppressed the diverse cytokine response seen in antigen-experienced Teff, Teff were isolated from human blood and activated in HPLM in the presence or absence of cana. Cana potently inhibited the secretion of key effector cytokines (IFNγ, IL-2, IL-4, IL-10, IL-17 and IL-21) at 24 h (Figure 6A), followed by a sustained suppression of most of these cytokines at 72 h (Figure 6B). Consistent with a critical role for cana in shaping activated Teff responses, we also saw a decrease in the master transcriptional regulators Tbet, GATA3, and RORγt (Figure 6C) concurrent with a striking reduction in blastogenesis that did not compromise viability (Figures 6D and S5A). Similar to our previous observations, activated Teff cultured with cana had reduced expression of activation markers CD25, CD44, and CD69 (Figure 6E).

One important effector CD4+ T cell population are Tregs. To determine the impact of cana on Treg biology we employed two approaches. Firstly, we sorted naive T cells and cultured them under Treg polarizing conditions for 6 days in the continuous presence of cana and determined FoxP3 expression. Here, treatment with cana did not significantly impact on FoxP3 expression (Figure S5B). Secondly, we polarized naive T cells toward the Treg compartment for 6 days and then re-stimulated differentiated Tregs for up to 72 h in the presence or absence of cana. Cana treatment did not significantly impact on FoxP3 expression at either time point (Figure S5C). We then assessed supernatant IL-10 levels of polarized Tregs cultured with cana for 24 h. In line with cana being a global T cell inhibitor, the presence of cana significantly impaired IL-10 production from Tregs (Figure S5D).

As cana significantly impacted on activated and effector T cell metabolism and function, we next questioned whether cana treatment possibly promoted T cell exhaustion by measuring expression of the co-inhibitory receptors LAG3, PD-1 and Tim-3 (Figure 6F). A negligible reduction in the expression of LAG3 and Tim-3 was seen, and a modest decrease in PD-1 expression. Here, our data indicate that cana is a global T cell inhibitor and its effects are mediated independently of T cell exhaustion.

Canagliflozin inhibits T cell function in systemic lupus erythematosus and rheumatoid arthritis

Thus far, we have demonstrated that cana is a global human T cell inhibitor, mechanistically disrupting both Myc- and mTORC1-driven programs leading to suppressed T cell metabolism and function. Therefore, cana may have significant potential as a repurposed drug for the treatment of T cell-mediated diseases. To this end, we isolated CD4+ T cells from two autoimmune patient cohorts (SLE and RA) and activated them for 24 h in the presence or absence of cana (Figure 7A). Strikingly, cana impaired cytokine production (IL-2 and IFNγ, Figures 7B and 7C, IL-17 and TNF; Figure S6A) and CD25, CD44, and CD69 expression (Figures 7D and 7E) but did not result in a decrease in T cell size (Figure S6B).

To account for the functional differences observed, we assessed whether the metabolic perturbations first observed in T cells from healthy donors upon cana treatment were recapitulated in T cells from patients with autoimmunity (Figures 5A–5D). Here, using extracellular flux analysis cana suppressed ECAR and both basal and maximal glycolytic rate (Figures S6C and S6E), in addition to decreasing ATP levels derived from glycolysis at both the basal and maximal rates (Figure S6F). In contrast, OXPHOS levels were impaired only at the maximal level, with basal levels unaffected (Figures S6G and S6G–S6I). We observed a significant decrease in the spare respiratory capacity of autoimmune T cells exposed to cana (Figure S6J), in addition

(J) Mass isotopolog distribution (MID) represented as a % pool of TCA cycle metabolites: α-ketoglutarate, citrate, fumarate, and malate of 8 h activated T cells. Numbers on the x axis represent the number of ^{13}carbons incorporated.

(K–N) (K) IL-2 production of CD4+ T cells activated with anti-CD3 (2 μg/mL) and anti-CD28 (20 μg/mL) for 24 h in the presence or absence of dimethyl 2-oxoglutarate (0.3 mM). Activated CD4+ T cells treated in the presence or absence of cana (10 μM), piericidin A (500 nM), R162 (10 μM), or combination of piericidin A and R162 with (L) extracellular IFNγ release, (M) CD69 expression, and (N) blastogenesis measured. CI, complex I.

Data are representative of nine (A–D), five (E, F, H, and L–N), four-five (I and J), or three (K) independent experiments. Data are expressed as mean ± SEM. See also Data S2.

Please cite this article in press as: Jenkins et al., Canagliflozin impairs T cell effector function via metabolic suppression in autoimmunity, Cell Metabolism (2023), https://doi.org/10.1016/j.cmet.2023.05.001

CellPress
OPEN ACCESS

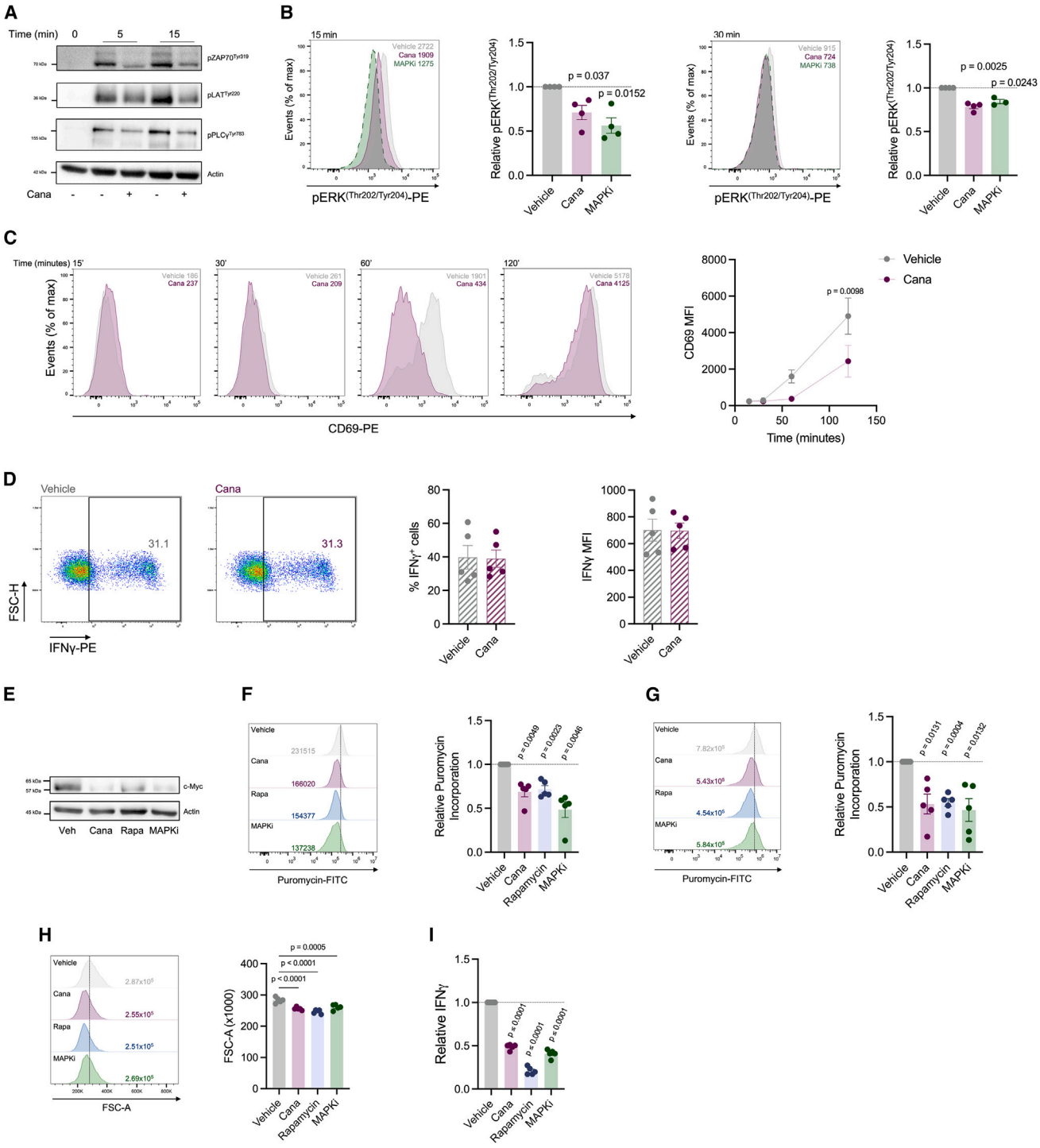

Figure 5. Canagliflozin impairs T cell receptor signaling

(A) CD4+ T cells activated with anti-CD3 (2 μg/mL) and anti-CD28 (20 μg/mL) for the indicated time points and downstream T cell receptor targets assessed by immunoblotting in the presence or absence of cana (10 μM).

(B) Relative expression of phosphorylated-ERK$^{Thr202/Tyr204}$ in anti-CD3 (2 μg/mL) and anti-CD28 (20 μg/mL) activated CD4+ T cells in the presence and absence of canagliflozin (10 μM), determined by flow cytometry for 15 and 30 min post-activation. MAP kinase inhibitor PD-98,059 (25 μM) used as a positive control. Representative overlaid histogram plots, numbers indicate median fluorescence intensity.

(C) Early expression of activation marker CD69 CD4+ T cells activated as (B) in the presence and absence of cana (10 μM), determined by flow cytometry.

(D) Intracellular cytokine staining of IFNγ in CD4+ T cells activated with PMA (10 ng/mL) and ionomycin (500 ng/mL) for 4 h.

(legend continued on next page)

Please cite this article in press as: Jenkins et al., Canagliflozin impairs T cell effector function via metabolic suppression in autoimmunity, Cell Metabolism (2023), https://doi.org/10.1016/j.cmet.2023.05.001

to a decrease in ATP levels derived from the maximal rate of OXPHOS (Figure S6K). Finally, to determine whether cana has an effect at the site of inflammation, we isolated and treated synovial fluid mononuclear cells (SFMNCs) from RA patients undergoing arthroscopy for 24 h (Figure 7F). Cana reduced TNF levels in 3 of the 4 patient samples and had a more profound effect decreasing IFNγ and IL-17 levels, with the latter reaching statistical significance (Figures 7G and 7I). Cana had a largely inhibitory effect on reducing activation markers CD25, CD44 and CD69 and cell size in both CD4+ and CD8+ T cells analyzed with one patient outlier in the CD4+ T cell subsets analyzed (Figures S7A–S7D). Interestingly, this patient had a lower CD4+ T cell compartment (17.5% of CD3 gated) compared with the other patients (average: 47.4%).

Importantly, these data reveal that cana retains its ability to potently suppress T cell responses in patients with autoimmunity, underlining cana as a critical modulator of T cell metabolism and effector function with significant potential for the treatment of T cell-mediated autoimmunity.

DISCUSSION

In this manuscript, we investigate repurposing two types of SGLT2 inhibitors as potential therapeutic options for T cell-mediated autoimmunity. Importantly, we demonstrate that using physiologically relevant doses, cana, but not dapa, significantly impairs human CD4+ T cell-mediated inflammation. Our data indicate that this is not due to inhibition of SLC5A2 or SGLT2, which is not expressed by T cells, rather by cana-specific effects impairing T cell signaling, metabolic perturbation, and downstream T cell-activation-induced remodeling.

We reveal that cana impacts on T cell activation by specifically blunting TCR signaling. This impaired TCR response led to compromised metabolic reprogramming and effector function; in part via inhibition of key metabolic nodes downstream of the TCR (mTORC1 and Myc) and in part via off-target effects of cana on GDH and complex I. Inhibition of GDH by cana led to impaired glutamine anaplerosis within the TCA cycle, demonstrated by decreased incorporation of glutamine-derived carbon into TCA cycle metabolites. T cells were, however, able to compensate by enhancing incorporation of glucose-derived carbon, notably within aspartate and glutamate pools. This is in line with the study by Wu et al., which showed that impaired aspartate pools led to the biogenesis of TNF in RA.[41] Second, antagonism of mitochondrial complex I by cana led to increased early mitochondrial ROS production concomitant with mitochondrial dysfunction.

Mechanistically, cana impaired early TCR signaling events ultimately compromising cytokine production. Interestingly, this observation could be rescued when stimulating T cells with PMA/ionomycin, thus bypassing the TCR. Reduced TCR transduction, mediated by cana, led to decreased ERK and mTOR, ultimately blunting c-Myc expression and activity. The observed decrease in mTORC1 signaling and reduced c-Myc expression at the protein level correlates with the compromised metabolic profile of T cells. Specifically, downstream metabolic targets of c-Myc that were suppressed in the presence of cana were of significant interest because of their association with glucose uptake (SLC2A1), glycolysis (HK2), one carbon metabolism (DHFR—also a specific target of the autoimmune drug, methotrexate) and fatty acid synthesis (ACLY and FASN). These data are in line with previous studies demonstrating the catastrophic effect on the T cell proteome of impaired c-Myc signaling.[39]

It is well known that aberrant T cell metabolism contributes to dysregulated function and breakdown of self-tolerance in autoimmunity.[42] Given the relative ineffectiveness alongside the crippling side-effects of certain autoimmune drugs, investigation into novel therapeutics is warranted. Multiple pre-clinical studies have demonstrated therapeutic benefit from targeting T cell metabolism in autoimmunity such as tetramization of the glycolytic enzyme pyruvate kinase,[43] inhibition of OXPHOS using oligomycin,[44] use of the glycolytic inhibitor 2-deoxy-D-glucose,[45] and glutaminase suppression.[46] However, while promising, the clinical translation of these studies remains a challenge due to the toxic nature of impairing metabolism at the whole-body level.

Interestingly, targeting immunometabolic processes using repurposed T2D drugs has previously demonstrated promise in multiple inflammatory disorders.[18,47] One of the most notable drug candidates is the complex I inhibitor metformin. In numerous studies, metformin has exhibited protective effects in a range of autoimmune disorders such as multiple sclerosis, SLE, and RA.[15,18,47] Aside from metformin, other T2D candidates have been investigated such as the PPAR-γ agonist, pioglitazone, again with promising results in reducing autoimmune-associated symptoms.[12,47]

The novel class of recently approved T2D medication, SGLT2 inhibitors, have extensive roles beyond improved glycemic control. Additional benefits include the ability of cana to elicit protective clinical outcomes in cardiovascular disease (CVD) and chronic kidney disease.[28,29] Furthermore, cana has been demonstrated to promote PD-L1 degradation by endocytic recycling in SGLT2 positive non-small cell lung cells.[48] Given these encouraging precedents, we sought to investigate the effects of SGLT2 inhibitors on human T cell function.

Critically, our results show that cana retained its ability to suppress T cell-mediated inflammation in two human *ex vivo* autoimmune cohorts—SLE and RA. Here, cana treatment led to the suppression of effector function in peripheral blood T cells (potentially preventing the repopulation of inflammatory T cells) and *ex vivo* synovial fluid mononuclear cells—further advocating the repositioning of cana to treat autoimmunity. A further benefit of prescribing patients with autoimmunity cana is the protective effects against CVD—a comorbidity causing significant morbidity and mortality in multiple autoimmune disorders.[49] Together, the impaired effector function of T cells accompanied by systemic protective effects against CVD highlights the exciting potential in repurposing cana for autoimmunity.

(E–I) (E) Immunoblot of c-Myc in CD4+ T cells activated for 4 h in the presence or absence of cana (10 μM), rapamycin (500 nM), or PD-98,059 (25 μM). Relative puromycin (10 μM) incorporation of T cells activated as (E) for (F) 4- and (G) 24 h. CD4+ T cells activated as (E) for 24 h with downstream (H) blastogenesis and (I) IFNγ measured.

Data are representative of four (A, B, and E), three (C), and five (D and F–I) independent experiments. Data are expressed as mean ± SEM.

See also Data S1 and S2.

Please cite this article in press as: Jenkins et al., Canagliflozin impairs T cell effector function via metabolic suppression in autoimmunity, Cell Metabolism (2023), https://doi.org/10.1016/j.cmet.2023.05.001

CellPress
OPEN ACCESS

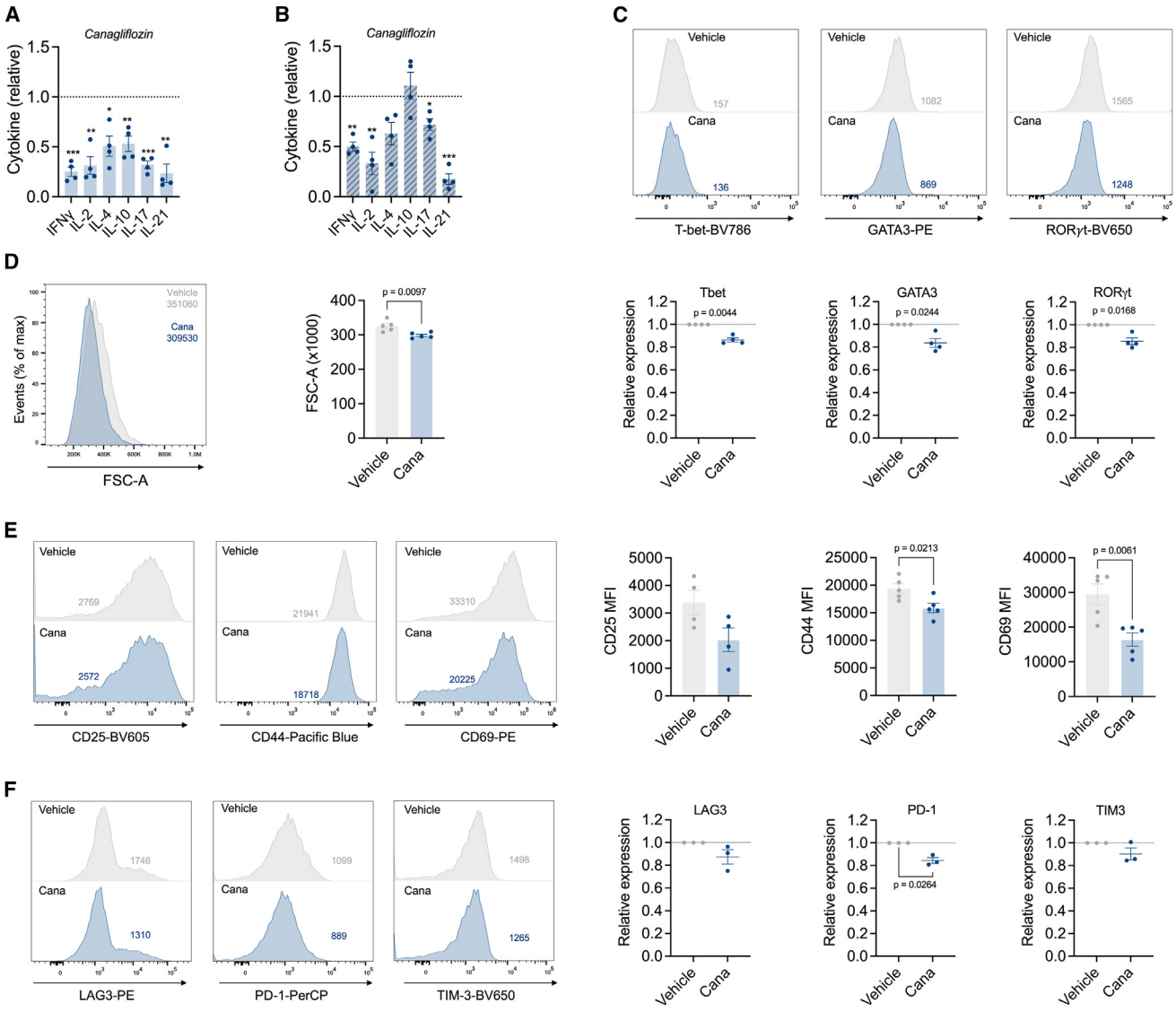

Figure 6. Canagliflozin limits Teff activation and effector function

(A and B) Extracellular cytokine release of IFNγ (p = 0.0005), IL-2 (p = 0.0045), IL-4 (p = 0.0164), IL-10 (p = 0.0092), IL-17 (p = 0.0004), and IL-21 (p = 0.0037) by anti-CD3 (2 μg/mL), and anti-CD28 (20 μg/mL) activated Teff at (A) 24 h and (B) 72 h activation IFNγ (p = 0.0410), IL-2 (p = 0.0056), IL-4 (p = 0.0277), IL-10 (p = 0.0044), IL-17 (p = 0.0005), and IL-21 (p = 0.0029).

(C) Relative expression of Th transcription factors Tbet, GATA3, and RORγt.

(D and E) (D) Teff blastogenesis and (E) expression of activation markers CD25, CD44, and CD69.

(F) Expression of exhaustion markers LAG3, PD-1, and TIM-3. Representative overlaid histogram plots, numbers indicate median fluorescence intensity or forward scatter-area.

Data are representative of four (A–C), five (D), four-five (E), or three (F) independent experiments. Data are expressed as mean ± SEM.

See also Data S2.

To conclude, a wealth of prior studies have reported that targeting T cell metabolism in autoimmunity can lead to therapeutic benefit. In our manuscript, we have demonstrated this by repurposing a clinically available T2D medication that modulates metabolism. Collectively, our manuscript demonstrates the inhibitory effects of cana on human CD4+ T cell function and provides a foundation for the clinical development of cana for the treatment of T cell-mediated autoimmune disease in humans.

Limitations of the study

Our study provides evidence in the repurposing of cana as a therapeutic intervention for T cell-mediated autoimmunity. RA is a complex and heterogeneous disease and further work is required to determine whether certain patient subgroups would preferentially benefit from cana therapy. It was beyond the scope of this study to investigate the impact of cana on other non-immune cell populations within the joint such as synovial fibroblasts and future work should determine whether inhibition of

Please cite this article in press as: Jenkins et al., Canagliflozin impairs T cell effector function via metabolic suppression in autoimmunity, Cell Metabolism (2023), https://doi.org/10.1016/j.cmet.2023.05.001

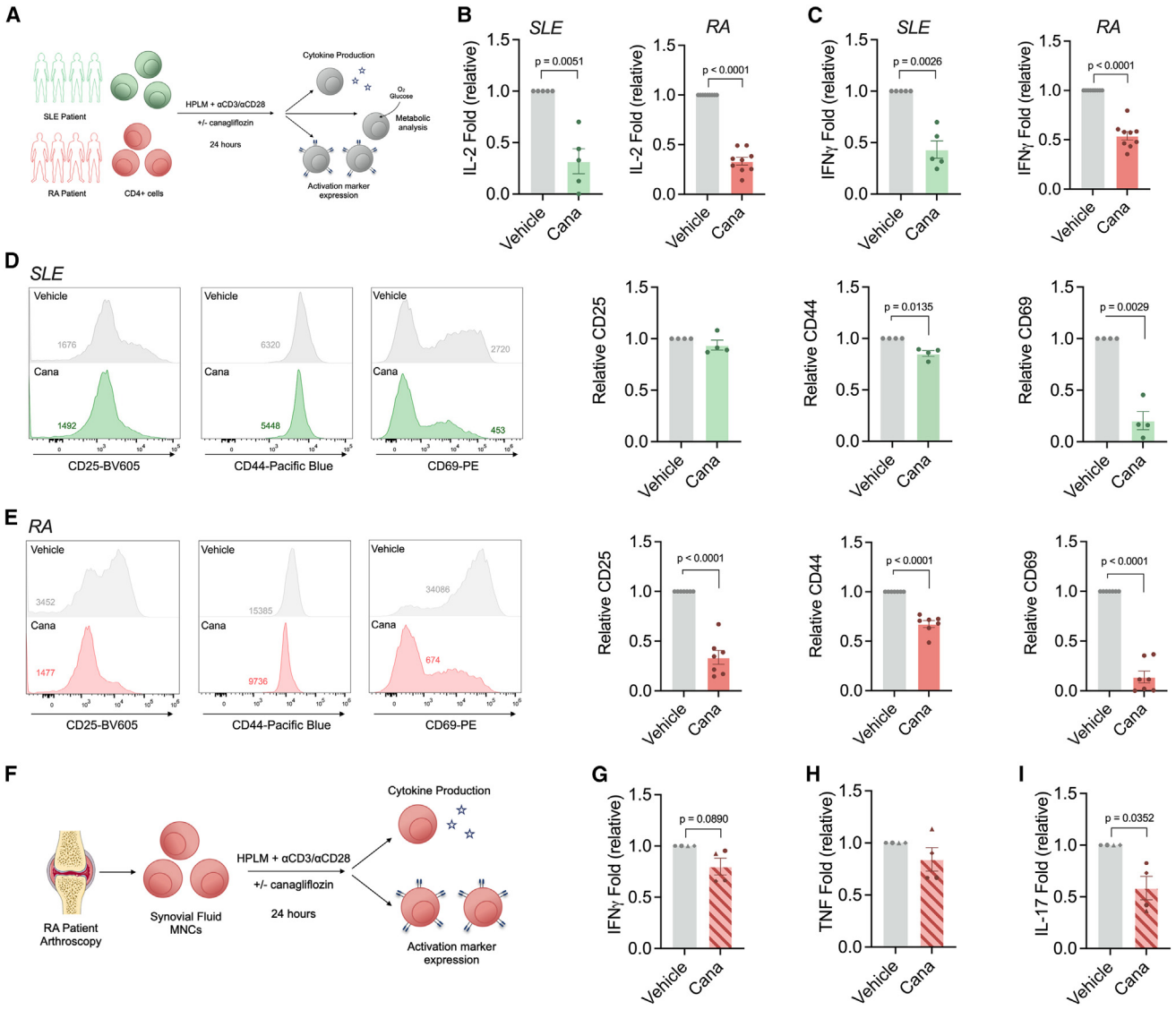

Figure 7. Canagliflozin inhibits T cell metabolism and effector function in patients with SLE or RA *ex vivo*

(A–E) (A) Schematic outlining the short-term experimental design of SLE (green) and RA-derived (red) T cells cultured in HPLM—anti-CD3 (2 μg/mL) and anti-CD28 (20 μg/mL) activated pan CD4+ T cells treated with or without canagliflozin (10 μM). Extracellular (B) IL-2 and (C) IFNγ release by SLE or RA pan CD4+ T cells. Expression of activation markers CD25, CD44, and CD69 in patients with (D) SLE or (E) RA. Representative overlaid histogram plots, numbers indicate median fluorescence intensity.

(F) Schematic of synovial fluid mononuclear cells (SFMNCs) isolated from an RA patient and treated with cana.

(G–I) (G) SFMNCs activated in HPLM with anti-CD3 (2 μg/mL) and anti-CD28 (20 μg/mL) for 24 h with TNF, (H) IFNγ or (I) IL-17 measured in the cell culture supernatant. Individual shapes correspond to an individual patient sample analyzed.

Data are representative of five-nine (B and C), four (D and G–I), or seven (E) independent experiments. Data are expressed as the mean ± SEM.

See also Data S2.

T cell inflammation by cana can reduce the inflammatory environment of the joint. Whether biologically relevant concentrations of cana would reach the inflamed joint is also a pertinent question and one that warrants further investigation. As cana is often prescribed in combination with metformin, it will therefore be poignant to determine whether there is a synergistic effect between the two drugs, potentially enhancing immunosuppressive capabilities in autoimmunity. Taken together, given that cana is an FDA-approved medication, a future clinical trial is warranted to determine whether cana has protective, clinical effects in patients with autoimmunity.

STAR★METHODS

Detailed methods are provided in the online version of this paper and include the following:

- KEY RESOURCES TABLE

Cell Metabolism
Clinical and Translational Report

CellPress
OPEN ACCESS

- RESOURCE AVAILABILITY
  - Lead contact
  - Materials availability
  - Data and code availability
- EXPERIMENTAL MODEL AND SUBJECT DETAILS
  - Human participants
  - Patient samples
  - Cell isolation and culture
- METHOD DETAILS
  - Alternative culture conditions
  - Human CD4+ regulatory T-cell differentiation
  - Enzyme-linked immunosorbent assay
  - Flow cytometry
  - Metabolic analysis
  - Immunoblotting
  - Stable Isotope Tracer Analysis (SITA) by LC-MS
  - RNA isolation
  - Nanostring nCounter® analysis
  - Proteomic analysis
  - Lactate assay
- QUANTIFICATION AND STATISTICAL ANALYSIS

SUPPLEMENTAL INFORMATION

Supplemental information can be found online at https://doi.org/10.1016/j.cmet.2023.05.001.

ACKNOWLEDGMENTS

We thank D.O.F. Skibinski, O. Bodger, A. Floudas, and S. Bain for useful discussion, A. Howden for proteomics advice, T. Jovic, E. Combellack, C. DeCourcey, K. Hawkins, and A. Tang for phlebotomy and all blood donors for their contribution to this work. B.J.J. is funded by a Swansea University Research Excellence Scholarship. G.W.J. is funded by a Versus Arthritis Career Development Fellowship (20305). J.B. was funded by a Canadian Institute for Health Research Postdoctoral Fellowship and the Kuok Family Postdoctoral Fellowship. E.E.V. is supported by a Diabetes UK RD Lawrence Fellowship (17/0005587) and by Cancer Research UK (C18281/A29019). This work was funded by a MRC New Investigator Research Grant (MR/X000095/1) awarded to N.J. We would like to acknowledge the FingerPrints Proteomics Facility at the University of Dundee, which is supported by the "Wellcome Trust Technology Platform" award (097945/B/11/Z). We thank the Metabolomics Facility at the Francis Crick Institute for their support.

AUTHOR CONTRIBUTIONS

B.J.J., J.B., F.M.P.-G., M.C., N.G., S.E., D.H., M.M.H., E.L.B., A.R., J.G.C., and N.J. performed experiments. B.J.J., J.B., E.H.M., D.K.F., S.K.D., L.V.S., G.W.J., E.E.V., and N.J. designed the experiments. B.J.J., J.B., D.H., S.E., E.L.B., S.K.D., G.W.J., E.E.V., and N.J. analyzed the data. E.C.J., D.J.V., and U.F. provided access to clinical samples. J.B., E.H.M., K.H.V., D.K.F., C.A.T., U.F., L.V.S., G.W.J., E.E.V., and N.J. provided intellectual discussion. B.J.J., E.E.V., and N.J. wrote the manuscript. All authors critically revised and approved the manuscript.

DECLARATION OF INTERESTS

K.H.V. is on the board of directors and shareholder of Bristol Myers Squibb, a shareholder of GRAIL, and on the science advisory board of PMV Pharma, RAZE Therapeutics, Volastra Pharmaceuticals, and Ludwig Cancer. She is a co-founder and consultant of Faeth Therapeutics, funded by Khosla Ventures. She has been in receipt of research funding from Astex Pharmaceuticals and AstraZeneca and contributed to CRUK Cancer Research Technology filing of patent application WO/2017/144877.

INCLUSION AND DIVERSITY

We support inclusive, diverse, and equitable conduct of research.

Received: August 4, 2022
Revised: February 3, 2023
Accepted: May 2, 2023
Published: May 24, 2023

REFERENCES

1. Jones, N., Vincent, E.E., Cronin, J.G., Panetti, S., Chambers, M., Holm, S.R., Owens, S.E., Francis, N.J., Finlay, D.K., and Thornton, C.A. (2019). Akt and STAT5 mediate naïve human CD4+ T cell early metabolic response to TCR stimulation. Nat. Commun. *10*, 2042. https://doi.org/10.1038/s41467-019-10023-4.
2. Gubser, P.M., Bantug, G.R., Razik, L., Fischer, M., Dimeloe, S., Hoenger, G., Durovic, B., Jauch, A., and Hess, C. (2013). Rapid effector function of memory CD8+ T cells requires an immediate-early glycolytic switch. Nat. Immunol. *14*, 1064–1072. https://doi.org/10.1038/ni.2687.
3. Jones, N., Cronin, J.G., Dolton, G., Panetti, S., Schauenburg, A.J., Galloway, S.A.E., Sewell, A.K., Cole, D.K., Thornton, C.A., and Francis, N.J. (2017). Metabolic adaptation of human CD4+ and CD8+ T cells to T cell receptor-mediated stimulation. Front. Immunol. *8*, 1516. https://doi.org/10.3389/fimmu.2017.01516.
4. Weyand, C.M., and Goronzy, J.J. (2017). Immunometabolism in early and late stages of rheumatoid arthritis. Nat. Rev. Rheumatol. *13*, 291–301. https://doi.org/10.1038/nrrheum.2017.49.
5. Buang, N., Tapeng, L., Gray, V., Sardini, A., Whilding, C., Lightstone, L., Cairns, T.D., Pickering, M.C., Behmoaras, J., Ling, G.S., et al. (2021). Type I interferons affect the metabolic fitness of CD8+ T cells from patients with systemic lupus erythematosus. Nat. Commun. *12*, 1980. https://doi.org/10.1038/s41467-021-22312-y.
6. Wu, B., Goronzy, J.J., and Weyand, C.M. (2020). Metabolic fitness of T cells in autoimmune disease. Immunometabolism *2*, e200017. https://doi.org/10.20900/immunometab20200017.
7. Yang, Z., Matteson, E.L., Goronzy, J.J., and Weyand, C.M. (2015). T cell metabolism in autoimmune disease. Arthritis Res. Ther. *17*, 29. https://doi.org/10.1186/s13075-015-0542-4.
8. Pucino, V., Certo, M., Bulusu, V., Cucchi, D., Goldmann, K., Pontarini, E., Haas, R., Smith, J., Headland, S.E., Blighe, K., et al. (2019). Lactate buildup at the site of chronic inflammation promotes disease by inducing CD4+ T cell metabolic rewiring. Cell Metab. *30*, 1055-1074.e8. https://doi.org/10.1016/j.cmet.2019.10.004.
9. Shan, J., Jin, H., and Xu, Y. (2020). T cell metabolism: a new perspective on Th17/Treg cell imbalance in systemic lupus erythematosus. Front. Immunol. *11*, 1027. https://doi.org/10.3389/fimmu.2020.01027.
10. McDonald, G., Deepak, S., Miguel, L., Hall, C.J., Isenberg, D.A., Magee, A.I., Butters, T., and Jury, E.C. (2014). Normalizing glycosphingolipids restores function in CD4+ T cells from lupus patients. J. Clin. Invest. *124*, 712–724. https://doi.org/10.1172/JCI69571.
11. Sun, F., Geng, S., Wang, H., Wang, H., Liu, Z., Wang, X., Li, T., Wan, W., Lu, L., Teng, X., et al. (2020). Effects of metformin on disease flares in patients with systemic lupus erythematosus: post hoc analyses from two randomised trials. Lupus Sci. Med. *7*. https://doi.org/10.1136/lupus-2020-000429.
12. Okunuki, Y., Usui, Y., Nakagawa, H., Tajima, K., Matsuda, R., Ueda, S., Hattori, T., Kezuka, T., and Goto, H. (2013). Peroxisome proliferator-activated receptor-γ agonist pioglitazone suppresses experimental autoimmune uveitis. Exp. Eye Res. *116*, 291–297. https://doi.org/10.1016/j.exer.2013.09.017.
13. Pershadsingh, H.A., Heneka, M.T., Saini, R., Amin, N.M., Broeske, D.J., and Feinstein, D.L. (2004). Effect of pioglitazone treatment in a patient with secondary multiple sclerosis. J. Neuroinflammation *1*, 3. https://doi.org/10.1186/1742-2094-1-3.

14. Neumann, B., Baror, R., Zhao, C., Segel, M., Dietmann, S., Rawji, K.S., Foerster, S., McClain, C.R., Chalut, K., van Wijngaarden, P., et al. (2019). Metformin restores CNS remyelination capacity by rejuvenating aged stem cells. Cell Stem Cell *25*, 473–485.e8. https://doi.org/10.1016/j.stem.2019.08.015.

15. Gharib, M., Elbaz, W., Darweesh, E., Sabri, N.A., and Shawki, M.A. (2021). Efficacy and safety of metformin use in rheumatoid arthritis: A randomized controlled study. Front. Pharmacol. *12*, 726490. https://doi.org/10.3389/fphar.2021.726490.

16. Naffaa, M.E., Rosenberg, V., Watad, A., Tiosano, S., Yavne, Y., Chodick, G., Amital, H., and Shalev, V. (2020). Adherence to metformin and the onset of rheumatoid arthritis: a population-based cohort study. Scand. J. Rheumatol. *49*, 173–180. https://doi.org/10.1080/03009742.2019.1695928.

17. Ursini, F., Russo, E., Pellino, G., D'Angelo, S., Chiaravalloti, A., De Sarro, G., Manfredini, R., and De Giorgio, R. (2018). Metformin and autoimmunity: a "new deal" of an old drug. Front. Immunol. *9*, 1236. https://doi.org/10.3389/fimmu.2018.01236.

18. Yin, Y., Choi, S.C., Xu, Z., Perry, D.J., Seay, H., Croker, B.P., Sobel, E.S., Brusko, T.M., and Morel, L. (2015). Normalization of CD4+ T cell metabolism reverses lupus. Sci. Transl. Med. *7*, 274ra18. https://doi.org/10.1126/scitranslmed.aaa0835.

19. Dziedzic, A., Saluk-Bijak, J., Miller, E., and Bijak, M. (2020). Metformin as a potential agent in the treatment of multiple sclerosis. Int. J. Mol. Sci. *21*. https://doi.org/10.3390/ijms21175957.

20. Nath, N., Khan, M., Paintlia, M.K., Singh, I., Hoda, M.N., and Giri, S. (2009). Metformin attenuated the autoimmune disease of the central nervous system in animal models of multiple sclerosis. J. Immunol. *182*, 8005–8014. https://doi.org/10.4049/jimmunol.0803563.

21. Cui, Y., Chang, L., Wang, C., Han, X., Mu, L., Hao, Y., Liu, C., Zhao, J., Zhang, T., Zhang, H., et al. (2019). Metformin attenuates autoimmune disease of the neuromotor system in animal models of myasthenia gravis. Int. Immunopharmacol. *75*, 105822. https://doi.org/10.1016/j.intimp.2019.105822.

22. Bapat, S.P., Whitty, C., Mowery, C.T., Liang, Y., Yoo, A., Jiang, Z., Peters, M.C., Zhang, L.J., Vogel, I., Zhou, C., et al. (2022). Obesity alters pathology and treatment response in inflammatory disease. Nature *604*, 337–342. https://doi.org/10.1038/s41586-022-04536-0.

23. National Institute for Health and Care Excellence (2016). Canagliflozin, dapaliflozin and empagliflozin as monotherapies for treating type 2 diabetes (TA390)*4*. https://www.nice.org.uk/guidance/ta390/resources/canagliflozin-dapagliflozin-and-empagliflozin-as-monotherapies-for-treating-type-2-diabetes-pdf-82602903454405.

24. Fray, J.C., Lush, D.J., Share, D.S., and Valentine, A.N. (1983). Possible role of calmodulin in renin secretion from isolated rat kidneys and renal cells: studies with trifluoperazine. J. Physiol. *343*, 447–454. https://doi.org/10.1113/jphysiol.1983.sp014903.

25. Mosley, J.F., Smith, L., Everton, E., and Fellner, C. (2015). Sodium-glucose linked transporter 2 (SGLT2) inhibitors in the management of type-2 diabetes: a drug class overview. P T *40*, 451–462.

26. Villani, L.A., Smith, B.K., Marcinko, K., Ford, R.J., Broadfield, L.A., Green, A.E., Houde, V.P., Muti, P., Tsakiridis, T., and Steinberg, G.R. (2016). The diabetes medication canagliflozin reduces cancer cell proliferation by inhibiting mitochondrial complex-I supported respiration. Mol. Metab. *5*, 1048–1056. https://doi.org/10.1016/j.molmet.2016.08.014.

27. Secker, P.F., Beneke, S., Schlichenmaier, N., Delp, J., Gutbier, S., Leist, M., and Dietrich, D.R. (2018). Canagliflozin mediated dual inhibition of mitochondrial glutamate dehydrogenase and complex I: an off-target adverse effect. Cell Death Dis. *9*, 226. https://doi.org/10.1038/s41419-018-0273-y.

28. Spertus, J.A., Birmingham, M.C., Nassif, M., Damaraju, C.V., Abbate, A., Butler, J., Lanfear, D.E., Lingvay, I., Kosiborod, M.N., and Januzzi, J.L. (2022). The SGLT2 inhibitor canagliflozin in heart failure: the CHIEF-HF remote, patient-centered randomized trial. Nat. Med. *28*, 809–813. https://doi.org/10.1038/s41591-022-01703-8.

29. Perkovic, V., Jardine, M.J., Neal, B., Bompoint, S., Heerspink, H.J.L., Charytan, D.M., Edwards, R., Agarwal, R., Bakris, G., Bull, S., et al. (2019). Canagliflozin and renal outcomes in Type 2 diabetes and nephropathy. N. Engl. J. Med. *380*, 2295–2306. https://doi.org/10.1056/NEJMoa1811744.

30. Heng, T.S.P., Painter, M.W., Elpek, K., Lukacs-Kornek, V., Mauermann, N., Turley, S.J., Koller, D., Kim, F.S., Wagers, A.J., and Asinovski, N. (2008). The Immunological Genome Project: networks of gene expression in immune cells. Nat. Immunol. *9*, 1091–1094. https://doi.org/10.1038/ni1008-1091.

31. Skapenko, A., Leipe, J., Lipsky, P.E., and Schulze-Koops, H. (2005). The role of the T cell in autoimmune inflammation. Arthritis Res. Ther. *7* (*Suppl 2*), 4–14. https://doi.org/10.1186/ar1703.

32. Tirmenstein, M., Dorr, T.E., Janovitz, E.B., Hagan, D., Abell, L.M., Onorato, J.M., Whaley, J.M., Graziano, M.J., and Reilly, T.P. (2013). Nonclinical toxicology assessments support the chronic safety of dapagliflozin, a first-in-class sodium-glucose cotransporter 2 inhibitor. Int. J. Toxicol. *32*, 336–350. https://doi.org/10.1177/1091581813505331.

33. Devineni, D., Curtin, C.R., Polidori, D., Gutierrez, M.J., Murphy, J., Rusch, S., and Rothenberg, P.L. (2013). Pharmacokinetics and pharmacodynamics of canagliflozin, a sodium glucose co-transporter 2 inhibitor, in subjects with type 2 diabetes mellitus. J. Clin. Pharmacol. *53*, 601–610. https://doi.org/10.1002/jcph.88.

34. Scheen, V. (2015). Pharmacodynamics, efficacy and safety of sodium-glucose co-transporter type 2 (SGLT2) inhibitors for the treatment of type 2 diabetes mellitus. Drugs *75*, 33–59. https://doi.org/10.1007/s40265-014-0337-y.

35. Leney-Greene, M.A., Boddapati, A.K., Su, H.C., Cantor, J.R., and Lenardo, M.J. (2020). Human plasma-like medium improves T lymphocyte activation. iScience *23*, 100759. https://doi.org/10.1016/j.isci.2019.100759.

36. Ramesh, R., Kozhaya, L., McKevitt, K., Djuretic, I.M., Carlson, T.J., Quintero, M.A., McCauley, J.L., Abreu, M.T., Unutmaz, D., and Sundrud, M.S. (2014). Pro-inflammatory human Th17 cells selectively express P-glycoprotein and are refractory to glucocorticoids. J. Exp. Med. *211*, 89–104. https://doi.org/10.1084/jem.20130301.

37. Salmond, R.J., Emery, J., Okkenhaug, K., and Zamoyska, R. (2009). MAPK, phosphatidylinositol 3-kinase, and mammalian target of rapamycin pathways converge at the level of ribosomal protein S6 phosphorylation to control metabolic signaling in CD8 T cells. J. Immunol. *183*, 7388–7397. https://doi.org/10.4049/jimmunol.0902294.

38. Wang, R., Dillon, C.P., Shi, L.Z., Milasta, S., Carter, R., Finkelstein, D., McCormick, L.L., Fitzgerald, P., Chi, H., Munger, J., et al. (2011). The transcription factor myc controls metabolic reprogramming upon T lymphocyte activation. Immunity *35*, 871–882. https://doi.org/10.1016/j.immuni.2011.09.021.

39. Marchingo, J.M., Sinclair, L.V., Howden, A.J., and Cantrell, D.A. (2020). Quantitative analysis of how Myc controls T cell proteomes and metabolic pathways during T cell activation. eLife *9*, e53725. https://doi.org/10.7554/eLife.53725.

40. Mak, T.W., Grusdat, M., Duncan, G.S., Dostert, C., Nonnenmacher, Y., Cox, M., Binsfeld, C., Hao, Z., Brüstle, A., Itsumi, M., et al. (2017). Glutathione primes T cell metabolism for inflammation. Immunity *46*, 675–689. https://doi.org/10.1016/j.immuni.2017.03.019.

41. Wu, B., Zhao, T.V., Jin, K., Hu, Z., Abdel, M.P., Warrington, K.J., Goronzy, J.J., and Weyand, C.M. (2021). Mitochondrial aspartate regulates TNF biogenesis and autoimmune tissue inflammation. Nat. Immunol. *22*, 1551–1562. https://doi.org/10.1038/s41590-021-01065-2.

42. Martins, C.P., and Piganelli, J.D. (2020). Targeting T cell metabolism to combat autoimmunity: implications for the future of type 1 diabetes therapeutics. Immunometabolism *2*, e200010. https://doi.org/10.20900/immunometab20200010.

43. Angiari, S., Runtsch, M.C., Sutton, C.E., Palsson-McDermott, E.M., Kelly, B., Rana, N., Kane, H., Papadopoulou, G., Pearce, E.L., Mills, K.H.G., et al. (2020). Pharmacological activation of pyruvate kinase M2 inhibits CD4+

T cell pathogenicity and suppresses autoimmunity. Cell Metab. *31*, 391–405.e8. https://doi.org/10.1016/j.cmet.2019.10.015.

44. Shin, B., Benavides, G.A., Geng, J., Koralov, S.B., Hu, H., Darley-Usmar, V.M., and Harrington, L.E. (2020). Mitochondrial oxidative phosphorylation regulates the fate decision between pathogenic Th17 and regulatory T cells. Cell Rep. *30*, 1898–1909.e4. https://doi.org/10.1016/j.celrep.2020.01.022.

45. Wilson, C.S., Stocks, B.T., Hoopes, E.M., Rhoads, J.P., McNew, K.L., Major, A.S., and Moore, D.J. (2021). Metabolic preconditioning in CD4+ T cells restores inducible immune tolerance in lupus-prone mice. JCI Insight *6*. https://doi.org/10.1172/jci.insight.143245.

46. Johnson, M.O., Wolf, M.M., Madden, M.Z., Andrejeva, G., Sugiura, A., Contreras, D.C., Maseda, D., Liberti, M.V., Paz, K., Kishton, R.J., et al. (2018). Distinct regulation of Th17 and Th1 cell differentiation by glutaminase-dependent metabolism. Cell *175*, 1780–1795.e19. https://doi.org/10.1016/j.cell.2018.10.001.

47. Negrotto, L., Farez, M.F., and Correale, J. (2016). Immunologic effects of metformin and pioglitazone treatment on metabolic syndrome and multiple sclerosis. JAMA Neurol. *73*, 520–528. https://doi.org/10.1001/jamaneurol.2015.4807.

48. Ding, L., Chen, X., Zhang, W., Dai, X., Guo, H., Pan, X., Xu, Y., Feng, J., Yuan, M., Gao, X., et al. (2023). Canagliflozin primes antitumor immunity by triggering PD-L1 degradation in endocytic recycling. J. Clin. Invest. *133*. https://doi.org/10.1172/JCI154754.

49. Schwartz, D.M., Burma, A.M., Kitakule, M.M., Luo, Y., and Mehta, N.N. (2020). T cells in autoimmunity-associated cardiovascular diseases. Front. Immunol. *11*, 588776. https://doi.org/10.3389/fimmu.2020.588776.

50. Mookerjee, S.A., Gerencser, A.A., Nicholls, D.G., and Brand, M.D. (2017). Quantifying intracellular rates of glycolytic and oxidative ATP production and consumption using extracellular flux measurements. J Biol Chem *292*, 7189–7207. https://doi.org/10.1074/jbc.M116.774471.

51. Wiśniewski, J.R., Hein, M.Y., Cox, J., and Mann, M. (2014). A "Proteomic Ruler" for Protein Copy Number and Concentration Estimation without Spike-in Standards. Mol Cell Proteomics *13*, 3497–3506. https://doi.org/10.1074/mcp.M113.037309.

Please cite this article in press as: Jenkins et al., Canagliflozin impairs T cell effector function via metabolic suppression in autoimmunity, Cell Metabolism (2023), https://doi.org/10.1016/j.cmet.2023.05.001

STAR★METHODS

KEY RESOURCES TABLE

REAGENT or RESOURCE	SOURCE	IDENTIFIER
Antibodies		
β-actin antibody	abcam	ab8226; RRID: AB_306371
4E-BP1 (53H11) antibody	Cell Signaling Technology	Cat#9644; RRID: AB_2097841
AMPKα antibody	Cell Signaling Technology	Cat#2532; RRID: AB_330331
c-Myc (D84C12) antibody	Cell Signaling Technology	Cat#5605; RRID: AB_1903938
CD3 human antibody (clone UCHT1)	Biolegend	Cat#300436; RRID: AB_2562124
CD3 human antibody (clone OKT3)	Biolegend	Cat#317326; RRID: AB_11150592
CD4 human antibody (clone OKT4)	Biolegend	Cat#317422; RRID: AB_571941
CD25 human antibody (clone BC96)	Biolegend	Cat#302631; RRID: AB_11123913
CD28 human antibody (clone CD28.2)	Biolegend	Cat#302943; RRID: AB_2166667
CD44 human antibody (clone BJ18)	Biolegend	Cat#338823; RRID: AB_2721612
CD45RA human antibody (clone HI100)	Biolegend	Cat#304134; RRID: AB_2563814
CD45RO human antibody (clone UCHL1)	Biolegend	Cat#304204; RRID: AB_314420
CD62L human antibody (clone DREG56)	Biolegend	Cat#304806; RRID: AB_314466
CD69 human antibody (clone FN50)	Biolegend	Cat#310906; RRID: AB_314841
CD69 human antibody (clone FN50)	Biolegend	Cat#310904; RRID: AB_314839
CD197 human antibody (clone G043H7)	Biolegend	Cat#353210; RRID: AB_10915695
ERK1/2 Phospho (Thr202/Tyr204) (clone 6B8B69)	Biolegend	Cat#369506; RRID: AB_2629705
FoxP3 human antibody (clone 206D)	Biolegend	Cat#320108; RRID: AB_492986
FoxP3 human antibody (clone 259D)	Biolegend	Cat#320216; RRID: AB_2104902
GATA3 human antibody (clone	Biolegend	Cat#653804; RRID: AB_2562722
IFNγ human antibody (clone 4S.B3)	Biolegend	Cat#502509; RRID: AB_315234
LAG3 human antibody (clone REA351)	Miltenyi	Cat#130-120-470; RRID: AB_2784078
Mouse secondary antibody	Cell Signaling Technology	Cat#7076S; RRID: AB_330924
PD1 human antibody (clone EH12.2H7)	Biolegend	Cat#329914; RRID: AB_1595461
Phospho-Acetyl-CoA Carboxylase (Ser79) antibody	Cell Signaling Technology	Cat#3661; RRID: AB_330337
Phospho-AMPKα (Thr172) antibody	Cell Signaling Technology	Cat#2535; RRID: AB_331250
Phospho-LAT (Tyr220) antibody	Cell Signaling Technology	Cat#3584; RRID: AB_2157728
Phospho-PLCγ1 (Tyr783) (D6M9S) antibody	Cell Signaling Technology	Cat#14008; RRID: AB_2728690
Phospho-S6 Ribosomal Proteins (Ser235/236) antibody	Cell Signaling Technology	Cat#2211; RRID: AB_331679
Phospho-Stat5 (Tyr694) antibody	Cell Signaling Technology	Cat#9351; RRID: AB_2315225
Phospho-Zap-70 (Tyr493)/Syk (Tyr526) antibody	Cell Signaling Technology	Cat#2704; RRID: AB_2217457
Puromycin human antibody	Merck	MABE343-AF488; RRID: AB_2736875
Rabbit secondary antibody	Cell Signaling Technology	Cat#7074S; RRID: AB_2099233
RORγT mouse antibody (clone Q21-559)	BD Biosciences	Cat#563424; RRID: AB_2738197
S6 Ribosomal Protein (5G10) antibody	Cell Signaling Technology	Cat#2217; RRID: AB_331355
Stat5 antibody	Cell Signaling Technology	Cat#9363; RRID: AB_2196923
Tbet mouse antibody (clone O4-46)	BD Biosciences	Cat#564141; RRID: AB_2738615
TIM3 human antibody (clone F38-2E2)	Biolegend	Cat#345028; RRID: AB_2565829
Biological samples		
Blood obtained from healthy adult donors	N/A	N/A
Blood obtained from rheumatoid arthritis patients	N/A	N/A

(*Continued on next page*)

Please cite this article in press as: Jenkins et al., Canagliflozin impairs T cell effector function via metabolic suppression in autoimmunity, Cell Metabolism (2023), https://doi.org/10.1016/j.cmet.2023.05.001

CellPress
OPEN ACCESS

Continued

REAGENT or RESOURCE	SOURCE	IDENTIFIER
Blood obtained from systemic lupus erythematosus patients	N/A	N/A
Synovial fluid obtained from rheumatoid arthritis patients	N/A	N/A
Chemicals, peptides, and recombinant proteins		
$^{13}C_5$-glutamine	Cambridge Isotopes	CLM-1396-PK
$^{13}C_6$-glucose	Cambridge Isotopes	CLM-1822-H-PK
Acetonitrile ≥99.9%, HiPerSolv CHROMANORM® for LC-MS, suitable for UPLC/UHPLC instruments	VWR	83640.290
Antimycin A	Merck	A8674
Canagliflozin	Cambridge Bioscience	CAY11575
Cell-Tak™ Cell and Tissue Adhesive	Corning	Cat#354240
Cleland's Reagent, ULTROL® Grade	Merck	233153
Dapagliflozin	Combi-Blocks	QE-4375
Dimethyl 2-oxoglutarate	Merck	349631
eBioscience™ Protein Transport Inhibitor Cocktail (500X)	Invitrogen	00-4980-93
Carbonyl cyanide-p-trifluoromethoxyphenylhydrazone (FCCP)	Merck	C2920
Formic Acid, 99.0+%, Optima™ LC/MS Grade, Fisher Chemical™	Fisher Scientific	10596814
Human IL-2 cytokine for stimulation	Miltenyi	130-097-745
Iodoacetamide	Merck	I6125
Ionomycin Calcium Salt	Merck	I3909
Lymphoprep™	StemCell Technologies	Cat#7861
Metformin hydrochloride	MedChemExpress	HY-17471A
Methanol ≥99.9% (by GC), HiPerSolv CHROMANORM® for LC-MS, suitable for UPLC/UHPLC instruments	VWR	83638.290
Monensin	Merck	M5273
Oligomycin	Merck	75351
Orthophosphoric acid ≥85%, AnalaR NORMAPUR® ACS, Reag. Ph. Eur. analytical reagent	VWR	20624.262
PD-98,059	Merck	513000
PhosphoSafe Extraction Buffer	Merck	71296
Pierce™ Formic Acid, LC-MS Grade	ThermoFisher	85178
Pierce™ Trypsin Protease, MS Grade	ThermoFisher	90057
Piericidin A	Enzo Life Sciences	ALX380235M002
PMA	Merck	79346
Puromycin	Merck	P7255
R162	Merck	5.38098
Rapamycin	Merck	553210
Rotenone	Merck	R8875
Sodium dodecyl sulfate	Merck	L4509
TGF-β	PeproTech	Cat#100-21
TMB Substrate Reagent Set	BD Biosciences	Cat#555214
Triethylammonium bicarbonate buffer	Merck	T7408
Water, HiPerSolv CHROMANORM® for LC-MS, suitable for UPLC/UHPLC instruments	VWR	83645.290

(*Continued on next page*)

Please cite this article in press as: Jenkins et al., Canagliflozin impairs T cell effector function via metabolic suppression in autoimmunity, Cell Metabolism (2023), https://doi.org/10.1016/j.cmet.2023.05.001

Continued

REAGENT or RESOURCE	SOURCE	IDENTIFIER
Critical commercial assays		
Acclaim PepMap 100 Å, 100 μm i.d. x 2cm NanoViper (2pk) - 164564	ThermoFisher	11312263
Acclaim PepMap C18 2um 75um x 500mm NVFS 1200bar - 164942	ThermoFisher	15567530
Acclaim PepMap RSLC C18, 2 μm, 100 Å, 75 μm i.d. x 15 cm - 164534	ThermoFisher	11342013
Amersham™ ECL Select™ Western Blotting detection reagent	Cytiva	RPN2235
CD4+ Effector Memory T cell isolation kit, human	Miltenyi	130-094-125
CD4+ T cell isolation kit, human	Miltenyi	130-096-533
CD8+ T cell isolation kit, human	Miltenyi	130-096-495
CellTrace™ Violet Cell Proliferation Kit, for flow cytometry	ThermoFisher	C34557
DC Protein Assay II	Bio-Rad	5000112
DRAQ7™	Biostatus	DR71000
ES791 - EASY-Spray 50cm x 20um Dual	ThermoFisher	15176864
ES800\A - EASY-Spray 15 cm x 75 μm	ThermoFisher	12886016 / 15988997
Human Granzyme B DuoSet ELISA	R&D Systems	DY2906
Human IFNγ DuoSet ELISA	R&D Systems	DY285B
Human IL-2 DuoSet ELISA	R&D Systems	DY202
Human IL-4 DuoSet ELISA	R&D Systems	DY204
Human IL-10 DuoSet ELISA	R&D Systems	DY217B
Human IL-17 DuoSet ELISA	R&D Systems	DY317
Human IL-21 DuoSet ELISA	R&D Systems	DY8879
Human TNFα DuoSet ELISA	R&D Systems	DY210
Immunocult T cell activator	StemCell Technologies	Cat#10971
Inside Stain Kit	Miltenyi	130-090-477
L-Lactate Assay Kit I	Eton Bioscience	Cat#120001200P
Micro BCA™ Protein Assay Kit	ThermoFisher	23235
MitoSOX™ Red	ThermoFisher	M36008
MitoTracker™ Green FM	ThermoFisher	M7514
Naïve CD4+ T cell isolation kit, human	Miltenyi	130-094-131
nCounter® Autoimmune Profiling Panel	Nanostring	XT-CSO-HAIP1-12
nCounter® Metabolic Pathways Panel	Nanostring	XT-CSO-HMP1-12
PepSwift Monolithic Capillary LC Columns - 164584	ThermoFisher	11382263
Pierce™ Quantitative Fluorometric Peptide Assay	ThermoFisher	23290
Restore™ PLUS Western Blot Stripping buffer	ThermoFisher	21063
RNeasy® Mini Kit columns	Qiagen	Cat#74014
SimplyBlue™ SafeStain	ThermoFisher	LC6060
TMRE-Mitochondrial Membrane Potential Assay Kit	abcam	Ab113852
Trifluoroacetic Acid, Optima™ LC/MS Grade, Fisher Chemical™	Fisher Scientific	10266617
Trypsin Sequencing Grade, modified	Merck	11418025001
Deposited data		
Raw data for Nanostring nCounter® Autoimmune Profiling Panel	NCBI Gene Expression Omnibus (GEO)	GSE228911; https://www.ncbi.nlm.nih.gov/geo/query/acc.cgi?acc=GSE228911
Raw data for Nanostring nCounter® Metabolic Pathways Panel	NCBI Gene Expression Omnibus (GEO)	GSE228911; https://www.ncbi.nlm.nih.gov/geo/query/acc.cgi?acc=GSE228911

(*Continued on next page*)

Please cite this article in press as: Jenkins et al., Canagliflozin impairs T cell effector function via metabolic suppression in autoimmunity, Cell Metabolism (2023), https://doi.org/10.1016/j.cmet.2023.05.001

CellPress
OPEN ACCESS

Continued

REAGENT or RESOURCE	SOURCE	IDENTIFIER
Raw data for Proteomics analysis	EMBL-EBI Proteomics Identification Database (PRIDE)	Identifier: PXD041523
Experimental models: Cell lines		
Human: PBMCs from healthy controls (primary)	N/A	N/A
Human: PBMCs from rheumatoid arthritis patients (primary)	N/A	N/A
Human: PBMCs from systemic lupus erythematosus patients (primary)	N/A	N/A
Human: SFMCs from rheumatoid arthritis patients (primary)	N/A	N/A
Software and algorithms		
ChemStation E.02.02.1431	Agilent	https://www.agilent.com/en/product/software-informatics/analytical-software-suite/chromatography-data-systems/openlab-chemstation
FlowJo 10.8.0	Tree Star	www.flowjo.com
GraphPad Prism 9	GraphPad Software, Inc.	www.graphpad.com
ImageJ	ImageJ	www.imagej.nih.gov/ij/
Morpheus	Broad Institute	https://software.broadinstitute.org/morpheus
NovoExpress 1.4.1	Agilent	https://www.agilent.com/en/product/research-flow-cytometry/flow-cytometry-software/novocyte-novoexpress-software-1320805
nSolver 4.0	Nanostring	www.nanostring.com/ncounterpro
Seahorse Wave Software 2.6	Agilent	https://www.agilent.com/en/product/cell-analysis/real-time-cell-metabolic-analysis/xf-software/seahorse-wave-desktop-software-740897
TraceFinder 4.1	ThermoFisher	https://www.thermofisher.com/uk/en/home/industrial/mass-spectrometry/liquid-chromatography-mass-spectrometry-lc-ms/lc-ms-software/lc-ms-data-acquisition-software/tracefinder-software.html
Other		
HBSS, no calcium, no magnesium, no phenol red	Gibco	14175053
Human plasma-like medium	Gibco	A4899101
RPMI 1640 Medium, GlutaMAX™ Supplement	Gibco	61870036
RPMI 1640 Medium, no glucose	Gibco	11879020
RPMI 1640 Medium, no glutamine	Gibco	31870025
Seahorse XF RPMI medium, pH 7.4	Agilent	103576-100
S-Trap™ mini columns (100 - 300 μg)	Protifi	CO2-mini-80
SeQuant ZIC-pHILIC, 5 micron, 150x4.6 mm	Merck	1.50461.0001

RESOURCE AVAILABILITY

Lead contact

Further information and requests for resources and reagents should be directed to and will be fulfilled by the lead contact, Nicholas Jones (n.jones@swansea.ac.uk).

Materials availability

This study did not generate new unique reagents.

Data and code availability

Nanostring nCounter® analysis data have been deposited at NCBI Gene Expression Omnibus (GEO: GSE228911) and are publicly available as of the date of publication. Proteomics analysis data have been deposited at EMBL-EBI Proteomics Identification

Database (ProteomeXchange: PXD041523) and are publicly available as of the date of publication. Accession numbers are listed in the key resources table. Original immunoblot images and raw data have been deposited in the Data S1. This paper does not report original code. Any additional information required to reanalyse the data reported in this paper is available from the lead contact upon request.

EXPERIMENTAL MODEL AND SUBJECT DETAILS

Human participants

Blood was obtained from healthy, non-fasted individuals. Individuals with infection or inflammatory conditions were excluded. Written informed contest was obtained by all participants according to ethical approval from Wales Research Ethics Committee (13/WA/0190).

Patient samples

Peripheral blood mononuclear cells (PBMCs) and synovial fluid mononuclear cells (SFMCs) were obtained from the cohort of rheumatoid arthritis (RA) patients. Written informed contest was obtained by all participants according to ethical approval from St. Vincent's University Hospital Ethics Committee (RS18-055).

PBMCs were obtained from the cohort of systemic lupus erythematosus (SLE) patients. Written consent was obtained by all participants according to ethical approval from London-Harrow Research Ethics Committee (11/LO/0330).

Demographic and clinical characteristics data of the study cohorts are presented in Tables S1 and S2.

Cell isolation and culture

PBMCs were isolated by density gradient centrifugation using Lymphoprep™ (StemCell Technologies). CD4+ and CD8+ T-cells were purified from human PBMCs by negative selection using automated magnetic cell separation (Miltenyi). Cells were cultured in human plasma like medium (HPLM; Gibco), unless otherwise stated, and activated in the presence of plate-bound anti-CD3 (2 μg/ml; Biolegend) and soluble anti-CD28 (20 μg/ml; Biolegend) or left unstimulated. Cultures were supplemented by 10% FBS following 3 h incubation to avoid impaired T cell activation. T-cells were treated with canagliflozin (Cambridge Bioscience) or dapagliflozin (Combi-Blocks) at a concentration of 10 μM, unless otherwise stated.

METHOD DETAILS

Alternative culture conditions

For certain experiments, IL-2 (10 ng/ml; Miltenyi) was added after 24 h. To bypass initial T cell receptor-dependent signalling, T-cells were activated using PMA (10 ng/ml; Merck) and ionomycin (500 ng/ml; Merck) for 4 h. For partial rescue, T-cells were activated in the presence and absence of canagliflozin, supplemented with dimethyl α-ketoglutarate (0.3 mM; Merck).

For complex I inhibition experiments, T-cells were activated in the presence or absence of rotenone (1 μM; Merck) or metformin hydrochloride (10 mM; MedChemExpress). High-dose metformin hydrochloride was used to bypass any transporter-specific uptake. For combined inhibition of complex I and glutamate dehydrogenase, T-cells were activated in the presence and absence of piericidin A (500 nM; Enzo Life Sciences) and R162 (10 μM; Merck).

To determine whether ERK inhibition or mTORC1 inhibition phenocopies canagliflozin treatment, T-cells were cultured in the presence of PD-98,059 (25 μM; Merck) and rapamycin (100 nM; Merck), respectively.

Human CD4+ regulatory T-cell differentiation

For regulatory T-cell (Treg) differentiation, naïve CD4+ T-cells were activated using Immunocult T cell activator (12 μl/ml; StemCell Technologies) and cultured with TGF-β (5 ng/mL; PeproTech) for 6 d in the presence and absence of canagliflozin (10 μM). Half of the medium was replaced at d3. At d6, cells were stained for FoxP3 (PE, mIgG1κ, 206D, 320108, Biolegend) and supernatants harvested. Additionally, Tregs induced in the absence of canagliflozin were restimulated (12 μl/ml; StemCell Technologies) at d6 in the presence and absence of canagliflozin before staining for FoxP3 at 24 h, 48 h and 72 h.

Enzyme-linked immunosorbent assay

Human IL-2 (DY202), IL-4 (DY204), IL-10 (DY217B), IL-17 (DY317), IL-21 (DY8879), IFNγ (DY285B), granzyme B (DY2906) and TNFα (DY210) were measured in cell-free culture supernatants according to the manufacturer's instructions (R&D Systems). ELISA plates were coated with the capture antibody and incubated overnight at 4°C. Wells were incubated at room temperature (RT) with gentle agitation with the following: appropriately-diluted cell-free supernatants and protein standards for 2 h, kit-specific detection antibody for 2 h, and streptavidin-horse radish peroxidase for 20 min. The plate was washed with 0.05% Tween-20 in PBS between each step. The plate was then incubated at RT with a 1:1 mixture of hydrogen peroxide and tetramethylbenzoic acid (BD Biosciences). Absorbance was measured at 450 nm after the addition of sulfuric acid (Merck) to each well and values were corrected to the blank.

Please cite this article in press as: Jenkins et al., Canagliflozin impairs T cell effector function via metabolic suppression in autoimmunity, Cell Metabolism (2023), https://doi.org/10.1016/j.cmet.2023.05.001

Flow cytometry

Flow cytometry analysis was performed on T-cells following culture. Cell death was monitored using DRAQ7™ (1 μM; Biostatus) and dead cells were excluded from analysis. Cell doublets were excluded based on forward scatter-height versus forward scatter-area. T-cell blastogenesis was assessed using forward scatter-area. Unless otherwise stated, surface and viability staining were performed for 15 min at RT in the dark.

CD4+ T-cell purity was verified using anti-CD3 (Brilliant Violet 570™, mIgG1κ, UCHT1, 300436) and anti-CD4 (AlexaFluor® 647, mIgG2b, OKT4, 317422). Naïve (Tnv) and effector (Teff) CD4+ T cell purity was measured using anti-CD4 (AlexaFluor® 647, mIgG2b, OKT4, 317422), anti-CD45RA (Brilliant Violet 605™, mIgG2b, HI100, 304134), anti-CD45RO (FITC, mIgG2a, UCHL1, 304204) and anti-CD197 (Pacific Blue, mIgG2a, G043H7, 353210) antibodies. Percentage purity was consistently > 90%.

Cell surface markers were monitored using the following antibodies: anti-CD3 (Brillian Violet 570™, mIgG1κ, UCHT1, 300436), anti-CD4 (Alexa Fluor® 647, mIgG2b, OKT4, 317422), anti-CD8 (PE, mIgG1κ, HIT8a, 300908), anti-CD25 (Brilliant Violet 605™, mIgG1κ, BC96, 302631), anti-CD25 (PE-Vio®615, rhIgG1, REA570, 130-123-035; Miltenyi), anti-CD44 (Pacific Blue™, mIgG1κ, BJ18, 338823), anti-CD62L (PE, mIgG1κ, DREG56, 304806), anti-CD69 (PE, mIgG1κ, FN50, 310906), anti-CD69 (FITC, mIgG1κ, FN50, 310904).

Intracellular markers were stained using the Inside Stain Kit (Miltenyi) as per the manufacturer's instructions. Following surface staining, cells were fixed for 20 min at RT before staining at RT for 10 min in the dark in permeabilisation buffer. Cells were stained for the following intracellular markers: anti-Tbet (Brilliant Violet 786™, mIgG1κ, O4-46, 564141; BD Biosciences), anti-GATA3 (PE, mIgG2b, 16E10A23, 653804), anti-RORγT (Brilliant Violet 650™, mIgG2b, Q21-559, 563424; BD Biosciences), anti-PD1 (PerCP/Cy5.5, mIgG1κ, EH12.2H7, 329914), anti-TIM3 (Brilliant Violet 650™, mIgG1κ, F38-2E2, 345028), anti-LAG3 (PE, recombinant IgG1, REA351, 130-120-470; Miltenyi), anti-ERK1/2 Phospho (Thr202/Tyr204; PE, mIgG2a, 6B8B69, 369506). For intracellular IFNγ staining, eBioscience Protein Transport Inhibitor Cocktail (Invitrogen) was added at the start of 4 h activation with PMA and ionomycin. Cells were stained overnight with anti-IFNγ (PE, mIgG1κ, 4S.B3, 502509) at 4°C in the dark in permeabilisation buffer.

For mitochondria content and membrane potential, cells were incubated with MitoTracker™ Green FM (100 nM; ThermoFisher) or TMRE (50 nM; abcam), respectively. For mitochondrial ROS staining, cells were incubated with MitoSOX™ Red (5 μM; ThermoFisher). All mitochondrial dyes were incubated for 20 min at 37°C.

CellTrace™ Violet Cell Proliferation kit (5 μM; ThermoFisher) was used to monitor T-cell proliferation. Cells were stained for 20 min in the dark prior to 72 h activation. Proliferation-associated parameters were calculated using the FlowJo Proliferation Platform (TreeStar).

Protein translation was assessed using anti-Puromycin (AlexaFluor® 488, 12D10, MABE343-AF488; Merck). Puromycin (10 μM; Merck) was introduced 15 min prior to the end of 4 h and 24 h T-cell activation. Cells were washed in ice-cold PBS before intracellular staining was performed using Inside Stain Kit (Miltenyi), whereby cells were fixed for 20 min at RT before 15 min permeabilisation. Finally, cells were stained at 4°C for 1 h in permeabilisation buffer.

Cells were acquired with Novocyte 3000 (Agilent), and analysis performed using FlowJo 10.8.0 or later (TreeStar). All antibodies purchased from (Biolegend, USA), unless otherwise stated.

Metabolic analysis

Metabolic analysis of T-cells was carried out using the Seahorse Extracellular Flux Analyzer XFe96 (Agilent). T-cells were activated for 24 hours with anti-CD3 (2 μg/mL; OKT3, Biolegend) and soluble anti-CD28 (20 μg/mL; CD28.2, Biolegend) in the presence or absence of the different SGLT2 inhibitors (10 μM). T-cells were resuspended in RPMI phenol red-free media containing 10 mM glucose, 2 mM glutamine and 1 mM pyruvate (Agilent). $2x10^5$ T-cells were seeded onto a Cell-Tak (354240; Corning) coated microplate allowing the adhesion of T-cells. Respiratory parameters (mitochondrial and glycolytic) were measured using OCR (pmoles/min) and ECAR (mpH/min), respectively, using injections: oligomycin (1 μM), FCCP (1 μM), rotenone and antimycin A (both 1 μM) and monensin (20 μM). All chemicals were purchased from Merck, unless stated otherwise. Metabolic parameters were calculated as per well-established protocols.[50]

Immunoblotting

T-cells were lysed using PhosphoSafe Extraction Buffer (Merck). Equivalent amounts of cell lysates proteins, as determined using DC Protein Assay (Bio-Rad), were denatured and separated using sodium dodecyl sulfate-polyacrylamide gel electrophoresis (SDS-PAGE). Proteins were transferred to polyvinylidene difluoride membranes using the Trans-Blot® Turbo™ transfer system as per the manufacturer's instructions. Following blocking in 5% BSA in TBST for 1 h at RT, membranes were probed overnight at 4°C with antibodies targeting the following: phospho-S6 ribosomal protein (2211), S6 ribosomal protein (2217), phospho-AMPKa (2535), AMPKa (2532), phospho-Acetyl CoA Carboxylase (3661), 4EBP1 (9644), phospho-STAT5 (9351), STAT5 (9363), c-Myc (5605), phospho-LAT (3584), phospho-PLCγ (14008) and phospho-ZAP70 (2704). Membranes were then incubated with HRP-conjugated anti-mouse or anti-rabbit antibodies for 1 h at RT (both Bio-Rad), washed three times in TBST, before incubation in Amersham™ ECL Select™ Western Blotting detection reagent (Cytiva) allowed visualisation of protein levels by enhanced chemiluminescence using the ChemiDoc™ XRS+ imaging system (Bio-Rad). Membranes to be re-analysed were immersed in Restore™ PLUS Western Blot stripping buffer (ThermoFisher) for 10 min to remove bound antibodies, before washing, blocking and incubated with the desired primary antibody, with the protocol continued as normal.

Please cite this article in press as: Jenkins et al., Canagliflozin impairs T cell effector function via metabolic suppression in autoimmunity, Cell Metabolism (2023), https://doi.org/10.1016/j.cmet.2023.05.001

All antibodies were purchased from Cell Signaling (Danvers, MA), unless otherwise stated, and used at a 1:1000 dilution. Protein loading was evaluated using β-actin (ab8226, Abcam).

Stable Isotope Tracer Analysis (SITA) by LC-MS

Isolated Tnv were incubated with universally heavy labelled $^{13}C_6$-glucose (11.1 mM; Cambridge Isotopes) in glucose free RPMI (ThermoFisher) or $^{13}C_5$-glutamine (2 mM; Cambridge Isotopes) in glutamine free RPMI (ThermoFisher). T-cells were activated with plate bound anti-CD3 (2 μg/mL; HIT3a, Biolegend) and free anti-CD28 (20 μg/mL; CD28.2, Biolegend) in the presence or absence of canagliflozin (10 μM) for a period of 8 h. Cells were then washed twice with ice cold PBS and lysed in 80% methanol. Cell extracts were then dried down at 4°C using a speed-vacuum concentrator. Samples were resuspended in acetylnitrate, methanol and water in a ratio of 50:30:20. The samples were subsequently analysed by LC-MS.

Metabolite analysis was performed by LC-MS using a Q-EXACTIVE Plus (Orbitrap) mass spectrometer (ThermoFisher) coupled with a Vanquish UHPLC system (ThermoFisher). The chromatographic separation was performed on a SeQuant® Zic®pHILIC (Merck) column (5 μm particle size, polymeric, 150 x 4.6 mm). The injection volume was 5 μL, the oven temperature was maintained at 25°C, and the autosampler tray temperature was maintained at 4°C. Chromatographic separation was achieved using a gradient program at a constant flow rate of 300 μl/min over a total run time of 25 min. The elution gradient was programmed as decreasing percentage of B from 80 % to 5 % during 17 minutes, holding at 5 % of B during 3 minutes and finally re-equilibrating the column at 80 % of B during 4 minutes. Solvent A was 20 mM ammonium carbonate solution in water supplemented by 4 ml/L of a solution of ammonium hydroxide at 35% in water and solvent B was acetonitrile. MS was performed with positive/negative polarity switching using a Q-EXACTIVE Plus Orbitrap (ThermoFisher) with a HESI II probe. MS parameters were as follows: spray voltage 3.5 and 3.2 kV for positive and negative modes, respectively; probe temperature 320°C; sheath and auxiliary gases were 30 and 5 arbitrary units, respectively; and full scan range: 70–1,050 m/z with settings of AGC target and resolution as balanced and high (3 × 106 and 70,000), respectively. Data were recorded using Xcalibur 4.2.47 software (ThermoFisher). Mass calibration was performed for both ESI polarities before analysis using the standard ThermoFisher Calmix solution. To enhance calibration stability, lock-mass correction was also applied to each analytical run using ubiquitous low-mass contaminants. Parallel reaction monitoring (PRM) acquisition parameters were the following: resolution 17,500; collision energies were set individually in HCD (high-energy collisional dissociation) mode. Metabolites were identified and quantified by accurate mass and retention time and by comparison to the retention times, mass spectra, and responses of known amounts of authentic standards using TraceFinder 4.1 EFS software (ThermoFisher).

RNA isolation

RNA isolation was performed using an RNeasy® Mini Kit as per the manufacturers' guidelines (all Qiagen, unless otherwise stated). Cells were lysed in a 1:1 solution of RLT buffer and 70% high-grade ethanol (Fisher Bioreagents, USA) and RNA bound to spin columns. Following several wash step, RNA was eluted in RNase-free water. The collected eluate was re-placed on the spin column membrane and centrifuged again to further increase the final concentration of the collected RNA. Purity was assessed using a NanoDrop™ spectrophotometer (ThermoFisher) by measuring the ratio of absorbance at 260 nm versus 280 nm or 230 nm. Measured A260/A280 and A260/A230 ratios were typically ~2.0. Any RNA samples with A260/230 ratio below 2.0 were precipitated using 0.3 M sodium acetate solution (ThermoFisher) and isopropanol. Subsequent measured A260/A230 ratios were typically improved to $\geq$ 2.0. Once purity was established, RNA was stored at -80°C until required for downstream analysis. Freeze-thaw cycles were avoided in order to prevent RNA degradation.

Nanostring nCounter® analysis

784 genes related to pathways and processes involved in autoimmune disease were analysed using the nCounter® Autoimmune Profiling Panel and 782 genes related to metabolic processes and signalling pathways were analysed using the nCounter® Metabolic Pathways Panel (NanoString). Target gene panels included positive controls, negative controls and housekeeping genes for quality control and normalisation. 50 ng of RNA was loaded per sample and hybridisation reactions were performed according to the manufacturer's instructions (Nanostring). Unique target-probe complexes were detected and scanned by the nCounter® SPRINT Profiler analysis system.

Raw data appraisal, quality control and normalisation were all performed using nSolver™ analysis software V4.0. The following criteria ensured sample quality control: imaging QC of >75% FOV registration, binding density QC within a range of 0.1 - 2.25, positive control linearity QC with R2 $\geq$ 0.95, and a positive control limit of detection QC set as 0.5 fM positive control above 2 standard deviations above the negative controls. Control and housekeeping genes were selected by the nSolver™ normalisation module and generated normalised data was used as input for further analysis.

For differential expression analysis, a $\log_2$ fold-change of $\leq$-1 or $\geq$1 and a p-value $\leq$ 0.05 determined differentially expressed genes. Pathway scores were calculated as the first principal component of the pathway genes' normalised expression. All p-values were adjusted using the Benjamini-Yekutieli method to control the false discovery rate (FDR).

Please cite this article in press as: Jenkins et al., Canagliflozin impairs T cell effector function via metabolic suppression in autoimmunity, Cell Metabolism (2023), https://doi.org/10.1016/j.cmet.2023.05.001

Proteomic analysis

Sample Processing

$2x10^6$ isolated Tnv were activated with anti-CD3 (2 μg/ml) and anti-CD28 (20 μg/ml) for 24 h. Cell pellets were washed in Hank's Balanced Salt Solution (Gibco) before storing at -80°C for proteomic analysis. Samples were resuspended to 200 μl with S-Trap lysis buffer (10% SDS, 100mM Triethylammonium bicarbonate) and sonicated for 15 min (30 s on, 30 s off, 100% Amplitude, 70% Pulse). After centrifugation the supernatant was transferred to fresh tubes and the proteins quantified using the Micro BCA Protein Assay (ThermoFisher). 150 μg of protein was processed using S-Trap mini columns (Protifi, #CO2-mini-80). The samples were digested overnight with 3.75 μg of trypsin (ThermoFisher, Pierce Trypsin Protease MS-Grade, #90057) with a second digest with the same amount of trypsin for 6 h the following day. Peptides were extracted and dried under vacuum. The peptides were then resuspended to 50 μl with 1% Formic Acid (ThermoFisher, #85178) and quantified using the Pierce Quantitative Fluorometric Peptide Assay (ThermoFisher, #23290).

Mass Spectrometry

Peptides (equivalent of 1.5 μg) were injected onto a nanoscale C18 reverse-phase chromatography system (UltiMate 3000 RSLC nano, ThermoFisher) and electrosprayed into an Orbitrap Exploris 480 Mass Spectrometer (ThermoFisher). For liquid chromatography the following buffers were used: buffer A (0.1% formic acid in Milli-Q water (v/v)) and buffer B (80% acetonitrile and 0.1% formic acid in Milli-Q water (v/v). Samples were loaded at 10 μL/min onto a trap column (100 μm × 2 cm, PepMap nanoViper C18 column, 5 μm, 100 Å, ThermoFisher) equilibrated in 0.1% trifluoroacetic acid (TFA). The trap column was washed for 3 min at the same flow rate with 0.1% TFA then switched in-line with a ThermoFisher, resolving C18 column (75 μm × 50 cm, PepMap RSLC C18 column, 2 μm, 100 Å). Peptides were eluted from the column at a constant flow rate of 300 nl/min with a linear gradient from 3% buffer B to 6% buffer B in 5 min, then from 6% buffer B to 35% buffer B in 115 min, and finally from 35% buffer B to 80% buffer B within 7 min. The column was then washed with 80% buffer B for 4 min. Two blanks were run between each sample to reduce carry-over. The column was kept at a constant temperature of 50oC. The data was acquired using an easy spray source operated in positive mode with spray voltage at 2.60 kV, and the ion transfer tube temperature at 250oC. The MS was operated in DIA mode. A scan cycle comprised a full MS scan (m/z range from 350-1650), with RF lens at 40%, AGC target set to custom, normalised AGC target at 300%, maximum injection time mode set to custom, maximum injection time at 20 ms, microscan set to 1 and source fragmentation disabled. MS survey scan was followed by MS/MS DIA scan events using the following parameters: multiplex ions set to false, collision energy mode set to stepped, collision energy type set to normalized, HCD collision energies set to 25.5, 27 and 30%, orbitrap resolution 30000, first mass 200, RF lens 40%, AGC target set to custom, normalized AGC target 3000%, microscan set to 1 and maximum injection time 55 ms. Data for both MS scan and MS/MS DIA scan events were acquired in profile mode.

Data Analysis

Analysis of the DIA data was carried out using Spectronaut (version 16.0.220606.53000, Biognosys, AG). Data was analysed using the directDIA workflow, with the following settings; imputation, profiling and cross run normalisation were disabledProtein LFQ Method was set to QUANT 2.0 (SN Standard) and Data Filtering to Qvalue; Precursor Qvalue Cutoff and Protein Qvalue Cutoff (Experimental) set to 0.01; maximum of 2 missed trypsin cleavages; PSM, Protein and Peptide FDR levels set to 0.01; cysteine carbamidomethylation set as fixed modification and acetyl (N-term), deamidation (asparagine, glutamine), oxidation of methionine set as variable modifications. The database used was the H.sapiens proteome downloaded from uniprot.org on 2021-05-11 (77,027 entries). Data filtering and protein copy number and concentration quantification was performed in the Perseus software package, version 1.6.6.0. Copy numbers were calculated using the proteomic ruler as described.[51] Further filtration of the data was completed to include proteins detected in at least $\geq$ 2 biological replicates, and exclude proteins identified based on single peptides. Samples were grouped according to the condition (activated or cana) to allow a comparison to be made between the control and treated samples. P values were calculated via a two-tailed, unequal-variance t-test on log-normalized data. Elements with P values < 0.05 were considered significant, with a fold-change cut-off > 1.5 or < 0.67. Heat maps were generated using the Morpheus tool from the Broad Institute (https://software.broadinstitute.org/morpheus). Mitochondrial complex proteins were identified using the following Gene Ontology Cellular Component terms: mitochondrial respiratory chain complex I (GO:0005747); mitochondrial respiratory chain complex III (GO:0005750); mitochondrial respiratory chain complex II, succinate dehydrogenase complex (ubiquinone) (GO:0005749); mitochondrial respiratory chain complex IV (GO:0005751); mitochondrial proton-transporting ATP synthase complex (GO:0005753).

Lactate assay

Extracellular L-lactate concentrations were measured using L-Lactate Assay Kit I (Eton Bioscience) as per the manufacturer's instructions. Cell-free supernatants were diluted to an appropriate concentration in dH_2O prior to the addition of L-Lactate Assay Solution and incubation at 37°C for 30 min. Absorbance was measured at 490 nm after the addition of 0.5M acetic acid (Merck) to each well and values were corrected to the blank.

Please cite this article in press as: Jenkins et al., Canagliflozin impairs T cell effector function via metabolic suppression in autoimmunity, Cell Metabolism (2023), https://doi.org/10.1016/j.cmet.2023.05.001

QUANTIFICATION AND STATISTICAL ANALYSIS

Statistical details of experiments can be found in the figure legends. All data are expressed as mean ± SEM as indicated in the figure legends. Statistical tests were selected based on appropriate assumptions with respect to data distribution and variance characteristics. For normally distributed data, statistical significance was determined using unpaired T test, one-way analysis of variance (ANOVA) followed by Dunnett's multiple comparisons test, or two-way ANOVA followed by Šidák's multiple comparisons test. For not normally distributed data, statistical significance was determined using Mann-Whitney test, or Kruskal-Wallis test followed by Dunn's multiple comparisons test. For data normalised to the vehicle control group, statistical significance was determined using one-sample T test. Any data involving a large number of multiple comparisons were adjusted for the FDR using the methods outlined. All statistical analyses were performed using GraphPad Prism 9.0. Significant differences are indicated as follows: * $p \leq 0.05$, ** $p \leq 0.01$, *** $p \leq 0.001$, **** $p < 0.0001$.